# Particle-Gas Dynamics and Primary Accretion

**Jeffrey N. Cuzzi**
*NASA Ames Research Center*

**Stuart J. Weidenschilling**
*Planetary Science Institute*

We review the basic physics of particle-gas interactions, and describe the various nebula epochs and regimes where these interactions are important. The potential role of turbulence is of special interest in a number of ways. Processes discussed include growth by sticking and incremental accretion, enhancement of abundance due to radial drift across evaporation boundaries, outward transport of small particles by diffusion and stellar winds, various midplane instabilities, and size-selective aerodynamic concentration of chondrule-sized particles. We provide examples of the structure and/or composition of primitive meteorites where these processes might have played a defining role, or where their signatures might be diagnostic.

## 1. OVERVIEW

It is likely that aerodynamic effects dominate the evolution of the main meteorite constituents (chondrules, refractory inclusions, fine-grained accretion rims, and matrix grains) into the first sizeable objects. We will refer to the first growth from free-floating nebula constituents to objects the size of meteorite parent bodies as primary accretion. In section 2, we review the underlying principles — the relevant properties of the nebula gas and its flow regimes, the physics of gas drag and particle stopping times, and the derivation of particle velocities in the presence or absence of turbulence. In section 3, we review the most well-developed incremental growth models for primary accretion, noting the role of sticking and how the growth regime changes as particles grow from fine dust to meters or larger. The key role of turbulence in determining growth timescales is first encountered here. In section 4, we describe a less-traditional path to primary accretion, in which turbulence selectively concentrates chondrule-sized constituents into dense zones that might subsequently evolve directly into objects with at least the mass of a many-meter-sized particle. In section 5, we note how solids can decouple from the gas and become widely redistributed, interacting with evaporation fronts in ways that can profoundly affect the regional mass distribution and chemistry of planet-forming materials. In section 6, we sketch an evolutionary scenario that might provide some helpful context for interpretation of the meteorite record. We summarize in section 7. Table 1 provides a list of symbols used frequently throughout this chapter.

## 2. UNDERLYING PRINCIPLES

### 2.1. The Nebula Gas

The properties of protoplanetary nebulae are as uncertain and controversial as those of meteorites. These are summarized in *Boss and Goswami* (2006) and *Russell et al.* (2006); see also the review by *Calvet et al.* (2000). The typical nebula mass M (98% hydrogen and helium) is a small fraction (0.02–0.2) of the stellar mass $M_*$, and cannot yet be measured directly. Current estimates of the surface gas mass density $\sigma_g(R)$ (g cm$^{-2}$), at distance R from the star, are based on assumptions about emission from solid particles, and will underestimate the disk mass once particles have grown past millimeter size. The concept of the minimum mass nebula (MMN) (e.g., *Hayashi,* 1981; *Hayashi et al.,* 1985) is a handy benchmark, but has no solid physical basis and (by construction) is an underestimate to the degree that solids were lost either into the Sun along with hydrogen, or by whatever subsequent processes depleted the asteroid region and ejected comets into the Oort cloud.

The nebula gas flows into the star at a rate $\dot{M}$ and velocity $V_n = \dot{M}/2\pi R\sigma_g$. The inflow rate $\dot{M}$, which decreases by orders of magnitude over the likely disk lifetime $M/\dot{M}$, also seems to vary by over an order of magnitude even for systems with the same apparent age (*Calvet et al.,* 2000) and thus the lifetime is both uncertain and probably system-dependent. Outward transport of angular momentum must occur to create this mass inflow. However, the mechanism for producing this transport is not well understood and remains a matter of debate. Turbulent viscosity $\nu_T$, once the mechanism of choice, has been questioned by many theorists in regions (such as the asteroid belt region) where the nebula gas is too dense and too cool to sustain a magnetorotational instability; this is primarily because numerical models of the differential rotation law obeyed by Keplerian disks have not demonstrated turbulent instability, and linear analysis does not predict it (*Stone et al.,* 2000). However, the situation regarding production of turbulence by differentially rotating neutral gas is in flux (e.g., *Richard and Zahn,* 1999; *Fleming and Stone,* 2003; *Richard,* 2003; *Mosqueira et al.,* 2003; *Klahr and Bodenheimer,* 2003a; *Arldt and Urpin,* 2004; *Umurhan and Regev,* 2004; *Garaud and Ogilvie,*

TABLE 1. List of frequently used symbols.

| Parameter | Definition |
|---|---|
| c | gas molecule thermal speed, or sound speed |
| C, $C_o$ | concentration or mass fraction of a tracer, and its cosmic value (section 5.4) |
| G | gravitational constant |
| $h_p$ | particle midplane layer vertical scale height (section 3.3.1) |
| H | nebula gas vertical scale height |
| $\ell$, L | generic, and largest, eddy scales in turbulence (section 2.2) |
| $M_\odot$ | solar mass |
| $M_*$ | stellar mass |
| $\dot{M}$ | nebula mass accretion rate, $M_\odot$/yr |
| r | particle radius |
| R | distance from the star |
| $R_{ev}$ | distance of an evaporation front from the star (section 5.4) |
| Re, Re* | turbulent Reynolds number (section 2); critical Re for midplane turbulence (section 3.3.1) |
| Ro | turbulent Rossby number of the near-midplane nebula gas (section 3.3.1) |
| St, $St_L$, $St_\eta$ | particle Stokes number = $t_s\Omega$, $t_s\Omega_L$, $t_s\Omega(\eta)$ (section 2.2) |
| $t_s$ | particle stopping time due to gas drag (section 2.2) |
| $V_K$ | Keplerian velocity |
| $V_L$ | "large" (typically, meter-sized) particle drift velocity ~ $\beta V_K$ (sections 2.3.1 and 5.4) |
| $V_n$ | nebula gas radial accretion velocity (sections 2.1 and 5.4) |
| $V_p$ | particle fluctuating velocity in turbulence (section 2.4) |
| $V_{pg}$ | relative velocity between particle and gas in turbulence (section 2.4) |
| $V_{pp}$ | relative velocity between identical particles in turbulence (section 2.4) |
| $\alpha$ | turbulent intensity parameter (section 2.1) |
| $\beta$ | pressure gradient parameter (section 2.3.1, $\eta$ of *Nakagawa et al.*, 1986) |
| $\mathcal{D}$, $\nu_T$ | nebula turbulent diffusivity and viscosity (section 2.1) |
| $\Delta V$ | maximum velocity difference or headwind between particles and gas (section 2.3.1) = $\beta V_K$ |
| $\eta$ | Kolmogorov scale; smallest eddy scale in turbulence (section 2.2) |
| $\nu_m$ | nebula gas molecular viscosity |
| $\Omega$ | angular velocity |
| $\Omega_K$ | Keplerian (orbital) angular velocity |
| $\Omega_L$ | largest eddy angular velocity |
| $\Omega_x$ | angular velocity at x-point near accreting star (section 5.1) |
| $\rho_s$ | individual particle internal density |
| $\rho_p$ | particle phase volume mass density |
| $\sigma_g$, $\rho_g$ | nebula gas surface and volume mass density |
| $\sigma_L$ | large particle surface mass density |

2005). Of special emerging interest is the possibility that even very small changes in some of the governing parameters, when extrapolated over the very large range of Reynolds numbers separating the nebula from current simulations, might lead to qualitatively different results (*Sreenivasan and Stolovitsky*, 1995a, and references therein; *Afshordi et al.*, 2005; *Mukhopadyay et al.*, 2005; also *Busse*, 2004).

Whatever the physics that drives nebular evolution, nebulae do evolve, and the ongoing inflow means that gravitational energy is constantly being released; this energy alone can maintain turbulent fluid motions. Some evidence for ongoing turbulence through the million-year timeframe is that disks of these ages, and older, commonly show evidence for small grains that are well distributed vertically (*Dullemond and Dominik*, 2005). Based only on the amount of energy being released by the evolving nebula, values of $\alpha \sim 10^{-5}$–$10^{-3}$ are not hard to justify (*Cuzzi et al.*, 2001). These fluid motions create a diffusivity $\mathcal{D}$ even if their particular correlations do not lead to a viscosity $\nu_T$ (cf. *Prinn*, 1990). We will finesse the distinction by taking their ratio, the Prandtl number Pr, equal to unity, and parameterize both $\mathcal{D}$ and $\nu_T$ by the dimensionless parameter $\alpha$: $\mathcal{D} = \nu_T = \alpha cH$, where c is the sound speed and H the nebula vertical scale height. Then $V_n \approx \nu_T/R$. Stellar winds and jets are observed in many, but not all, systems, and their strengths generally decrease along with $\dot{M}$ (*André et al.*, 2000).

The nebula gas is heated by a combination of stellar radiation and local dissipation of the released gravitational energy $GM_*\dot{M}/R$. The relative strength of these energy sources depends on the actual viscous dissipation and the steepness of flaring of the vertical scale height H(R). Infrared observations of disk thermal emission can be related to gas temperatures at various vertical and radial locations by making assumptions about the opacity of the solids in the nebula, which is a function of their (time-variable, and mostly unknown) particle size. The temperature is higher near the star, and (if viscous heating is important) closer to the midplane, but just where and when the temperature

reaches interesting values such as the condensation points of refractory oxides, silicates, or water ice is model dependent and might have varied from one system to another. For any given $\dot{M}$, nebula temperatures are higher for smaller $\alpha$ (the disk must be more massive) and run higher in recent models and analyses (*Papaloizou and Terquem,* 1999; *Bell et al.,* 1997; *Woolum and Cassen,* 1999) than those reviewed in the original volume of this series (*Wood and Morfill,* 1988).

Nebula models are usually described by their gas density $\rho_g = \sigma_g/2H$; however, meteoriticists usually prefer pressure. The conversion is simply done using the ideal gas law $P = \rho_g R_g T/\mu = \rho_g c^2/3$, where $R_g = 8.3 \times 10^7$ erg/mole-°K = 82.1 $cm^3$ atm/mole-°K is the universal gas constant, $\mu = 2$ g/mole for molecular hydrogen, local T is degrees Kelvin, and local $\rho_g$ is g/$cm^3$.

For the purpose of this chapter we will adopt a canonical nebula, keeping in mind that key parameters such as the mass M, turbulent intensity parameter $\alpha$, and lifetime M/$\dot{M}$ of our own nebula are uncertain by at least an order of magnitude. We will subsequently discuss how different values of M and/or $\dot{M}$ might relate to different nebula epochs, radial regimes, and mineral products. For a specific example, take a MMN accreting at $\dot{M} = 10^{-7}$ $M_\odot$/yr (*Bell et al.,*1997). At 3 AU, with a temperature of 500 K and $\rho_g = 10^{-10}$ g/$cm^3$, $P = 2 \times 10^{-6}$ bar. At 0.3 AU with a temperature of 1500 K and $\rho_g = 3 \times 10^{-8}$g/$cm^3$, $P = 1.8 \times 10^{-3}$ bar (see also *Wood,* 2000). Densities and pressures might have been higher in the early days of the nebula (<$10^6$ yr) when formation of refractory inclusions occurred, and lower by the classical T Tauri stage when $\dot{M}$ probably dropped to $10^{-8}$ $M_\odot$/yr (*Woolum and Cassen,* 1999).

### 2.2. Particle Stopping Times and Turbulent Eddy Times

The particle stopping time $t_s$ is the time in which the particle equilibrates with a gas moving at some relative velocity. Small, light particles have short stopping times and adjust much more quickly to gas fluctuations than large, dense particles. Particle-gas coupling is by a drag force, which depends on the gas density $\rho_g$, the particle radius r, and its internal density $\rho_s$ (which is lower than the "solid" density for porous aggregates such as fluffy CAIs). If the particle radius is larger than the molecular mean free path $\lambda \approx 50$ ($10^{-10}$ g $cm^{-3}/\rho_g$) cm, $t_s$ can depend on its relative velocity as well. Full descriptions of the various regimes of interest are given by *Weidenschilling* (1977), *Nakagawa et al.* (1986), and *Cuzzi et al.* (1993). Since the gas mean free path even at 1 AU is several centimeters, all typical constituents of chondrites satisfy $r < \lambda$, so we will generally use the so-called Epstein drag stopping time expression

$$t_s = \frac{r\rho_s}{c\rho_g} \qquad (1)$$

For particles with $r > \lambda$ (the Stokes drag regime), up to nearly 10 m radius under nebula conditions, $t_s$ remains nearly velocity-independent and may be approximated by multiplying the expression above by the factor $r/2\lambda$ (*Cuzzi et al.,* 1993).

In the case of a turbulent gas, particles experience constantly fluctuating velocity perturbations from eddies with a range of length scales $\ell$ and associated fluctuation times $t_e(\ell)$. Turbulence is an essentially lossless cascade of energy from large, slowly rotating eddies with lengthscale L and velocity $V_g$, which are forced by nebula-scale processes, through smaller and smaller scales, with correspondingly faster eddy timescales, to some minimum lengthscale $\eta$, called the Kolmogorov scale, where molecular viscosity $\nu_m$ can dissipate the macroscopic gas motions and turbulence ceases. Instead of presuming that large eddy scales L are on the order of the scale height H, which leads to $V_g = c\alpha$, we believe it more realistic to presume that large eddy frequencies $\Omega_L$ are no slower than the orbit frequency $\Omega_K$ due to coriolis effects; this logic leads to $V_g = c\alpha^{1/2}$ and $L = H\alpha^{1/2}$ (for details see *Shakura et al.,* 1978; *Cuzzi et al.,* 2001). This relationship for $V_g(\alpha)$ differs from that presented by *Shakura and Sunyaev* (1973), and subsequently followed by a number of authors, including *Weidenschilling and Cuzzi* (1993); thus turbulent velocities are larger than previously thought for any given $\alpha$, with implications for settling and diffusion of particles from chondrule size to meter size (sections 3 and 5). The turbulent Reynolds number is $Re = (L/\eta)^{4/3}$ (*Tennekes and Lumley,* 1972), where for canonical nebula parameters at 3 AU $Re = \alpha cH/\nu_m \sim 3 \times 10^7$ for $\alpha = 10^{-4}$. In this case, using $L = H\alpha^{1/2}$, $\eta \sim LRe^{-3/4} \sim$ 1 km. In most known cases of real turbulence, the Kolmogorov energy spectrum is a good approximation. Then, for a wide range of lengthscales $\eta < \ell < L$, the turbulent kinetic energy density $E(\ell)$ is given by the inertial range expression $E(\ell) = (V_g^2/2L)(\ell/L)^{-1/3}$, where the factor $V_g^2/2L$ is obtained from the normalization $\int_\eta^L E(\ell)d\ell = V_g^2/2$. The energy characterizing a typical lengthscale $\ell$ is $E(\ell,d\ell = \ell) = \ell E(\ell) = \ell(V_g^2/2L)(\ell/L)^{-1/3} = 0.5\ V_g^2(\ell/L)^{2/3}$. Then the eddy frequencies for arbitrary $\ell$ scale as $\Omega(\ell) = 1/t_e(\ell) = v(\ell)/\ell = (2\ell E(\ell))^{1/2}/\ell = \Omega_L(\ell/L)^{-2/3}$ (e.g., cf. *Tennekes and Lumley,* 1972; *Cuzzi et al.,* 1996, 2001).

In calculating the response of a particle to fluctuating eddy motions of this type, the dimensionless Stokes number $St = t_s\Omega(\ell)$ is used. Particles with $St \ll 1$ with respect to some eddy scale $\ell$ have stopping times much less than the overturn time $\Omega(\ell)^{-1}$ and are strongly coupled to those eddies. Particles with $t_s$ much less than even the shortest (Kolmogorov eddy) overturn time $t_e(\eta)$ are coupled to the gas and, effectively, move as gas molecules. In most cases we will define $St = St_L = t_s\Omega_L = t_s\Omega_K$; however, in section 4 we describe interesting and relevant effects associated with particles having stopping time $t_s$ equal to $t_e(\eta) = \Omega_K^{-1}(\eta/L)^{2/3} = \Omega_K^{-1}(Re^{-3/4})^{2/3} = \Omega_K^{-1}Re^{-1/2}$.

### 2.3. Meteorite Observations Implicating Aerodynamics

*Dodd* (1976) first discovered evidence for aerodynamic sorting in unequilibrated ordinary chondrites (UOCs). He com-

pared the sizes of metal grains, and silicate grains of different metal content, and found that the sizes and densities were consistent with $r\rho_s$ = constant (cf. equation (1)). Shortly thereafter, *Hughes* (1978) determined, from thin section and disaggregation analysis, that complete, rounded chondrules and obvious fragments of larger chondrules obeyed the same size distribution. This was reemphasized by *Leenhouts and Skinner* (1991) and *Skinner and Leenhouts* (1991), who also noted the presence of pre-accretionary fine-grained dust rims on chondrule fragments. They concluded that aerodynamics operating on solid particles, rather than something about the formation process, was deterministic to the characteristic narrow chondrule size distributions. *Scott and Haack* (1993) obtained similar results for Lancè (CO3). *Nelson and Rubin* (2002) commented that chondrule fragments in Bishunpur (LL3) were notably smaller than whole chondrules in Bishunpur; however, their Table 2 reveals that chondrules and fragments generally cover the same size range, with aerodynamic differences possibly attributable to shape. As did *Dodd* (1976) for UOCs, *Skinner and Leenhouts* (1993) showed that metal and silicate particles from Acfer 059 (CR2) had the same $r\rho_s$. *Hughes* (1980) found that the density and diameter of disaggregated silicate chondrules were inversely correlated; similarly, *Cuzzi et al.* (1999) found that, for disaggregated chondrules for which both r and $\rho_s$ could be measured, distribution histograms narrowed if the correct $r\rho_s$ product were used for each chondrule. *Kuebler et al.* (1999) introduced tomographic techniques and found that metal grains (although irregularly shaped) and silicate chondrules in three UOCs have nearly the same $r\rho_s$. Consistent with their more irregular shapes, the metal grains of *Kuebler et al.* (1999) were less well sorted than the more equidimensional chondrules. *Haack and Scott* (1993) have suggested that aerodynamical sorting of high-FeO and low-FeO chondrules might have been responsible for the differences between the UOC types (more-dense, low-FeO chondrules sorted primarily into the H chondrites). In sections 4 and 6.3, we describe newer, possibly diagnostic results regarding turbulent concentration of aerodynamically selected particles, and acquisition of fine-grained dust rims, in nebula turbulence.

Not all meteorites and components are so simply interpreted, however. Calcium-aluminum-rich inclusion sizes are poorly known (*May et al.*, 1999) but CAIs appear to be less narrowly sorted (and also somewhat larger) than chondrules and chondrule fragments in the same chondrites. Perhaps this is due to fluffiness, irregular shapes, or lower material densities of the CAIs. However, the chondrite types having the smallest (largest) chondrules also tend to have the smallest (largest) CAIs, supportive of aerodynamic sorting (*Scott et al.*, 1996). It is also true that in CH and CB chondrites, the metal particles are as large, or larger, than the silicate particles (A. Meibom, unpublished data, 2000; personal communication, 2003; see, e.g., *Greshake et al.*, 2002, Fig. 1). This latter fact, if indeed true, seems to be incompatible with aerodynamic sorting. It is emerging that CH and CB chondrites are the youngest of all chondrites (*Amelin et al.*, 2002, 2004; *Krot et al.*, 2005a; *Bizarro et al.*, 2004), and they may have formed in very different environments than normal chondrules and chondrites (*Connolly et al.*, 2006; *Weisberg et al.*, 2006). For more discussion of meteoritic constraints on the environment of these small particles, see *Cuzzi et al.* (2005a).

### 2.4. Particle Velocities

As one simple example of how $t_s$ works, under a nonfluctuating acceleration such as that due to the vertical component of solar gravity $g_z(z) = -\Omega_K^2 z$, particles reach a terminal velocity $V_z = g_z t_s$, which is size dependent through $t_s(r)$ and altitude dependent through both $g_z$ and $t_s(\rho_g(z))$. Below, we expand on how particles respond to the forces that act upon them; first we discuss the case without turbulence, and then show how turbulence (fluctuating acceleration) affects things.

*2.4.1. The headwind and radial drift.* *Whipple* (1972) first pointed out that the nebula gas can rotate either more slowly or more rapidly than the Keplerian velocity of a solid particle, depending on the local pressure gradient. The general decrease of gas density and temperature with increasing distance from the Sun, and the corresponding outward pressure gradient, provide a slight outward acceleration on the gas that opposes the dominant inward acceleration of solar gravity. Solid particles, responding only to solar gravity, experience a headwind from the more slowly rotating gas, which saps their angular momentum, causing them to orbit more slowly than the local Keplerian velocity and to drift inward. Subsequent work by *Adachi et al.* (1976), *Weidenschilling* (1977), and *Nakagawa et al.* (1986) describes this physics very clearly and it is only paraphrased here.

The ratio of the differential pressure gradient acceleration $\Delta g$ to the dominant central gravity acceleration g is

$$\beta \equiv \frac{\Delta g}{2g} = \frac{dP/dR}{2\Omega_K^2 R\rho_g} \sim 10^{-3} - 10^{-2} \qquad (2)$$

in the asteroid belt region, where the range in $\beta$ is due to the uncertain range of radial density and temperature gradients in the nebula (see *Cuzzi et al.*, 1993, Table 1). A useful approximation is that $\beta \approx (c/V_K)^2 \approx (H/R)^2$.

A parcel of gas experiencing an outward pressure gradient characterized by $\beta$ will orbit at a velocity slower than Keplerian by an amount $\Delta V = \beta V_K$; at 2.5 AU, $V_K$ = 18 km/s, so $\Delta V \sim$ 36–144 m/s. Large bodies ($\gg$1 m) are not significantly influenced by the gas and orbit at Keplerian velocity, thus incurring a headwind of this magnitude. The very smallest particles are forced to orbit at the gas velocity, but do not feel the outward gas pressure acceleration, so have an imbalance of gravitational and centrifugal accelerations $\Delta g = 2\beta R\Omega_K^2 = 2\beta\Omega_K V_K$. These particles drift slowly inward under this constant acceleration at terminal radial velocity $V_R = \Delta g t_s = 2St\beta V_K = 2St\Delta V$. Radial drift rates increase with size through increasing $t_s$, and this expression is actually quite good over a wide range of particle sizes <30 cm or so. Particles of roughly meter size, with $t_s \approx t_e(L) = 1/\Omega_K$, expe-

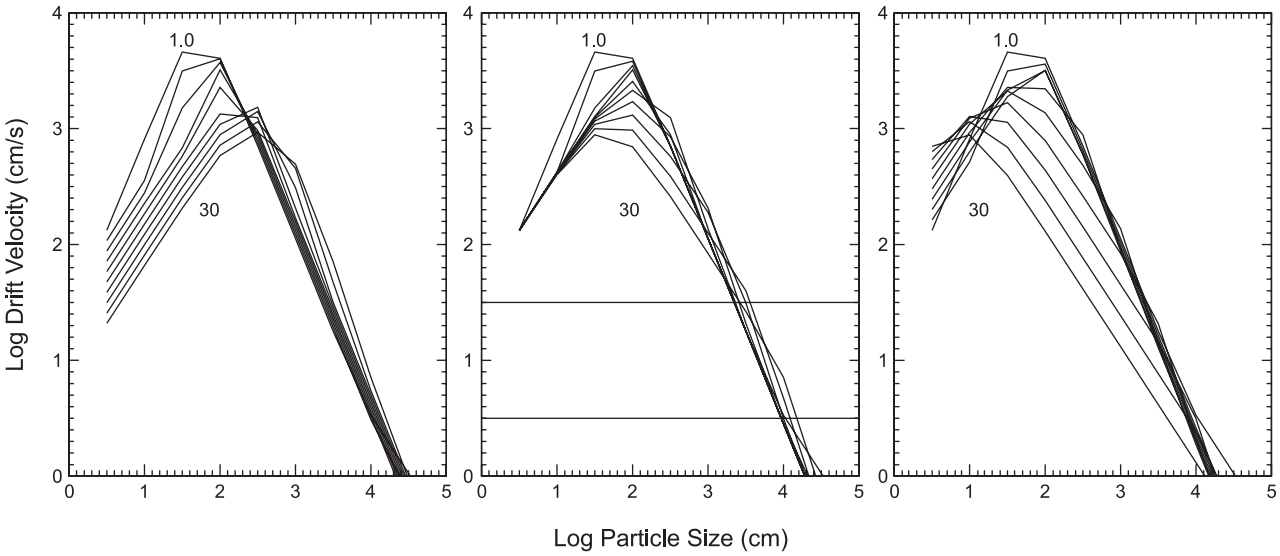


**Fig. 1.** Radial (inward) drift velocity for unit density particles at different locations in a nominal nebula model ($\sigma_g = 1700(1\ AU/R)^{-p}$ g $cm^{-2}$), as functions of particle radius (cm) and distance from the Sun (AU). Left: p = 1/2; center: p = 1; right: p = 3/2. For comparison, the horizontal band in the p = 1 plot indicates the range of nebula gas advection, or inward drift, velocities $V_n$ due to angular momentum transport at 5 AU from the Sun for a typical model with $\alpha = 10^{-3}$ (sections 2.1 and 2.4.1). Curves are labeled at radii of 1 and 30 AU, and at equal factors of 1.4 between.

rience nearly the full headwind yet are not massive enough to avoid drifting; they achieve the maximum radial drift rate $V_R \approx \Delta V$ (*Weidenschilling,* 1977). An example of radial drift velocities $V_R$ for a range of nebula models is shown in Fig. 1. Over this range, gas densities decrease radially outward, leading to an outwardly increasing $t_s$ that partially offsets the outwardly decreasing $V_K$; thus radial dependence of $V_R$ is not particularly strong (especially for $\sigma_g \propto R^{-1}$).

As the local particle mass density $\rho_p$ grows, such as near the midplane, particles with $\rho_p \geq \rho_g$ can drive the entrained gas toward Keplerian velocity, which decreases their headwind and drift rates $V_\theta$ and $V_R$ (see below). Analytical expressions for all particle headwind and drift velocities relative to the gas have been derived by *Nakagawa et al.* (1986) for arbitrary ratios of local particle mass density to gas mass density. These can conveniently be used in the limit $\rho_p/\rho_g \ll 1$ to obtain headwinds and drift velocities for isolated particles of any size and density.

We note that drift velocities are systematic, and depend on particle size. Identical particles would have the same velocity components and no relative velocity; they would experience no collisions due to drift. If turbulence is present, it can produce relative velocities and collisions between identical particles (as well as those of different sizes). Unless the nebula is perfectly laminar, particle velocities will be due to both sources, with the actual values dependent on nebular parameters, turbulence properties, and particle sizes.

*Local pressure fluctuations and particle concentrations:* Even though the nebula has an overall outward pressure gradient, strong local effects might arise in which pressure gradients, and particle drift, could go both ways. For instance, particles could quickly drift *into* local radial pressure maxima in the nebula gas (*Haghighipour and Boss*, 2003a,b; *Fromang and Nelson,* 2005; *Johansen et al.,* 2005). If the nebula gas is globally gravitationally unstable, large-scale spiral density waves will provide such localized nearly radial pressure maxima. Transient local enhancement in spiral density waves of the most rapidly drifting (meter-sized) particles by factors of 10–100 has been seen (*Rice et al.*, 2004). The end result is similar to that seen associated with large vortices (section 3.3.3) in that some potential for particle mass density enhancements exists. As discussed in section 3.3.3, increased collision rates in these regions may or may not lead to faster particle growth, depending on the relative collisional velocities, which will be connected to the strength of turbulence associated with these large-scale fluid dynamical structures (*Boley et al.,* 2005).

*2.4.2. Particle velocities in turbulence.* While particle velocities in turbulence have been studied extensively in the fluid dynamics literature (see *Cuzzi and Hogan,* 2003), the first and main contribution in the astrophysics literature was made by *Völk et al.* (1980, hereafter *VJMR*). It was updated by *Markiewicz et al.* (1991, hereafter *MMV*), who included the importance of the cutoff in turbulent forcing at the Kolmogorov scale $\eta$ as suggested by *Weidenschilling* (1984), and also studied by *Clarke and Pringle* (1988).

We will refer to particle velocities with respect to inertial space as $V_p$, those with respect to the gas (combined radial and angular components) as $V_{pg}$, and those with respect to each other as $V_{pp}$. In general, $V_p$ is used to determine the diffusive nature of particle motions, and plays a role in determining the thickness of the midplane particle layer and thus the planetesimal growth rate (section 3.3), as well as diffusing small particles such as CAIs and chondrules ra-

dially throughout the nebula (section 6.2). $V_{pg}$ determines how fast the particle sweeps through the gas (and smaller particles more firmly tied to the gas), and plays a role in constraining how chondrules and CAIs acquire fine-grained accretion rims (section 6.3). $V_{pp}$ determines how often like particles encounter each other and with what collisional speed (section 3.3.2). *Cuzzi and Hogan* (2003) expand on the *VJMR* prescription and derive simple, fully analytical expressions for $V_p$, $V_{pg}$, and $V_{pp}$ for arbitrary (identical) particles in turbulence of arbitrary intensity. An alternate derivation, but restricted to $V_p$, was presented by *Cuzzi et al.* (1993).

The response of a particle to turbulence, which has a spectrum of eddy scales and frequencies, is much like the classical problem of the response of an oscillator to periodic forces of different frequency. The oscillator responds well to forces that vary more slowly than its natural response time, and poorly to those that vary more rapidly. For a particle, the natural response time is just $t_s$. Particles will simply be entrained in eddies that have overturn time $>t_s$, and will share their velocities and spatial excursions. However, nearby, identical size particles in the same eddy will obtain almost no *relative* velocity from these eddies. Particles do experience random perturbations, in different directions, from smaller eddies with smaller timescales than $t_s$, and even nearby particles can incur random relative velocities this way. However, the absolute velocities of small, high-frequency eddies are smaller than for large, low-frequency ones (section 2.2). So small particles have slow relative velocities, and those with $t_s$ smaller than the smallest eddy overturn time have only very small relative velocities (section 3.2).

Figure 2 shows $V_p$, $V_{pg}$, and $V_{pp}$ for (identical) particles of a wide range of sizes, in turbulence of three different Re (or $\alpha$). All are normalized by the turbulent gas velocity $V_g = c\alpha^{1/2}$. The particle size is presented on the lower axis in full generality as the Stokes number $St_L = t_s/t_L$ where $t_L$ is the overturn time of the largest eddy — presumed to be the local orbit period. Very roughly, centimeter-radius, unit density particles at 2.5 AU from the Sun in a standard MMN have $t_s \sim 10^5$ s and thus $St_L \sim 3 \times 10^{-3}$. It is of special note that meter-radius particles have $t_s \sim$ orbit period and thus $St \sim 1$.

Several points of interest are shown in this figure. There is a single curve for $V_p$, because only the largest eddies contribute to $V_p$ and so the value of Re, which essentially determines the size of the Kolmogorov scale $\eta$ and its eddy properties, is unimportant. Particles of all sizes up to nearly a meter share a significant fraction of the gas turbulent velocity. The particle diffusion coefficient $\mathcal{D}_p$, which we will use in section 3.3 to calculate the density of midplane particle layers, and in section 6.2 to explain the preservation of CAIs for millions of years after their formation, can be written as $\mathcal{D}_p = \mathcal{D}V_p^2/V_g^2 = \mathcal{D}/(1 + St)$ (*VJMR*; *Cuzzi et al.*, 1993; *Cuzzi and Hogan*, 2003). Recent numerical studies are generally in agreement with these predictions (*Schräpler and Henning*, 2004; *Carballido et al.*, 2005), Second, for large particles, $V_{pp}$ decreases with size as $St_L^{-1/2}$; for particles smaller than $St_L \approx 1$, $V_{pp}$ increases with size as $St_L^{1/2}$; however, $V_{pp}$ drops sharply to zero for particles with $St_L < Re^{-1/2}$, which translates into particles having $t_s < t_e(\eta)$. We will use $V_{pp}$ in section 3.3.2 to calculate the collisional destruction time of meter-sized particles. Third, there is a steepening in slope of $V_{pg}$ for particle sizes with $t_s < t_e(\eta)$. We will use $V_{pg}$ to model the thickness of fine-grained accretion rims on chondrules and CAIs in section 6.3.

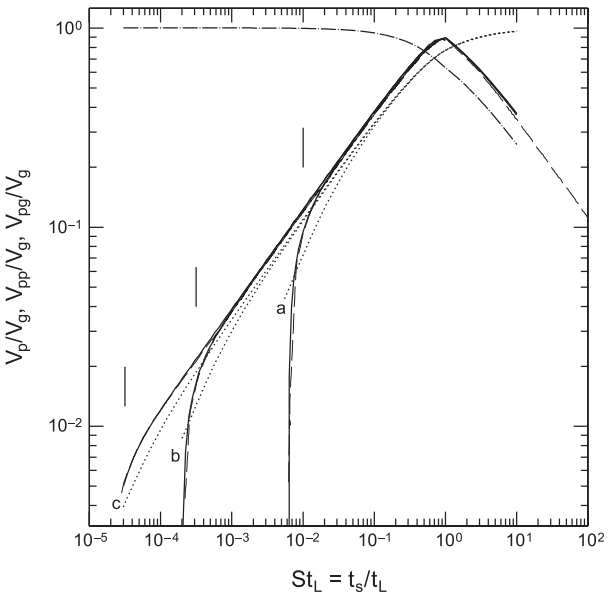


**Fig. 2.** $V_p$ (dot-dash), $V_{pg}$ (dotted), and $V_{pp}$ (solid) for (identical) particles of a wide range of sizes, as normalized by the gas turbulent velocity $V_g$, and in turbulence of three different Re (or $\alpha$). (a) Re = $10^4$; (b) Re = $10^7$; (c) Re = $10^9$. Dashed curve = exact numerical solutions from *MMV*; vertical hash marks = location where $St_\eta = 1$ (discussed in section 4). Figure from *Cuzzi and Hogan* (2003).

## 3. INCREMENTAL GROWTH

### 3.1. Sticking

The preceding discussion of particle velocities makes it clear that their relative motions lead to collisions. Even in a nonturbulent nebula, differential drift velocities are typically larger than the escape velocity for bodies smaller than about a kilometer, so growth must involve nongravitational sticking. This requires an attractive force between particles, such as van der Waals or other forms of surface energy, electrostatic or magnetic forces, and some mechanism of dissipating energy during a collision. Outcomes of collisions depend on the impact velocities and the absolute and relative sizes of the particles, along with their physical properties, such as density, impact strength, surface energy, elastic modulus, etc. The result may be sticking, rebound, net gain or erosional loss of mass, or disruption (*Blum*, 2004). For a thorough review of recent progress, see *Dominik et al.* (2006).

Theoretical analyses of collisional mechanics are limited to idealized spherical particles and aggregates thereof. *Chokshi et al.* (1993) considered head-on collisions of spherical particles, with dissipation of energy by elastic vibrations, and derived a critical velocity for the transition between sticking and rebound. The analysis was extended by *Dominik and Tielens* (1997) to include energy dissipation by sliding, twisting, and rolling of contact points between particles; they derived criteria for growth, restructuring, and disruption of aggregates. The theory of *Dominik and Tielens* (1997) predicts that two particles of radius r have a critical velocity for sticking

$$V_{stick} \sim \frac{2(\mathcal{E}/r)^{5/6}}{E^{1/3}\rho_s^{1/2}} \quad (3)$$

where $\mathcal{E}$ is the surface energy and E is Young's modulus. For properties of quartz, this expression gives $V_{stick} \sim 2 \times 10^{-3}$ (r/1 cm)$^{-5/6}$ cm s$^{-1}$. A micrometer-sized grain would stick to another grain (or the surface of a much larger body such as a chondrule) at an impact velocity <5 cm s$^{-1}$. For chondrule-sized particles (r = 0.05 cm), $V_{stick} \sim 0.025$ cm s$^{-1}$. *Blum* (2000) performed laboratory experiments on dust aggregation, and found sticking velocities about an order of magnitude larger than predicted by this theory for the measured values of elastic constants and surface energy. This difference might be due to electrostatic binding, nonsphericity of grains, or other factors. The transition between sticking and fragmentation occurs at around 1 m/s, with some nonzero sticking probability for velocities exceeding 10 m/s. Irregular micrometer-sized grains stick with efficiency of about 50% even at relative velocities greater than 10 m/s (*Blum*, 2004). Particles in the solar nebula probably were softer than silica, with lower elastic moduli. Thus, micrometer-sized grains in the solar nebula should coagulate readily, and chondrules can acquire a coating of grains due to van der Waals bonding alone (section 6.3). Additional sticking forces, such as electrostatic or magnetic interactions, may have been present, but were not necessary.

Collision velocities between chondrule-sized particles depend on the turbulent intensity $\alpha$ and the gas density $\rho_g$ (Fig. 2). Even if these velocities preclude sticking of individual, solid, chondrule-sized particles by van der Waals forces, electrostatic forces might play a role. *Marshall and Cuzzi* (2001) and *Marshall et al.* (2005) presented microgravity studies of chondrule-sized silicate particles that show no tendency at all to stick under terrestrial conditions — much like the familiar "dry grains of sand on a beach" analogy suggests. Under microgravity conditions, tribocharging generates dipole moments on these particles that make them stick quite readily to each other, sometimes forming large dust bunnies having net dipole moments that actively attract nearby particles, and are stable to being bumped up against their containers at speeds of tens of centimeters per second or more. The nebula conditions under which triboelectric (collisional) charging balances charge leakage to the nebula are not at all understood, but a high particle concentration may be needed (see *Desch and Cuzzi*, 2000). Further studies of the sticking of aggregates under microgravity conditions would be valuable.

### 3.2. Early Growth of Small Aggregates

The following discussion assumes nominal nebular parameters at 3 AU, with temperature 500 K, density $10^{-10}$ g cm$^{-3}$, and turbulence characterized by $\alpha = 10^{-4}$ (Re = $3 \times 10^7$). The largest eddies have velocity scale $V_g \sim c\alpha^{1/2} \sim 2 \times 10^3$ cm s$^{-1}$. From the relations in section 2.2, the smallest eddies have scales of size, velocity, and time on the order of 1 km, 25 cm/s, and 1 h, respectively. Consider an initial population of grains with radius 0.5 μm (mass m ~ $10^{-12}$ g), having abundance $3 \times 10^{-3}$ times that of the gas. The response time to the gas (equation (1)) is $t_s \sim 5$ s, much less than the large eddy timescale, so $St_L \sim 10^{-7}$. From Fig. 2, it is apparent that relative velocities due to turbulence would be negligible for identical particles. However, collisions at this scale are driven by thermal motions. Particles have thermal velocities $V_{th} = (8\,kT/\pi m)^{1/2} \sim 0.4$ cm/s, from which one can show that the mean collision time is about 10 yr. The collision velocity is less than the threshold for perfect sticking, so grains would coagulate to form fractal structures of low density (*Kempf et al.*, 1999). For simplicity we assume the fractal dimension is 2, which leads to the density of an aggregate being inversely proportional to its radius (mass proportional to the square of the radius). The thermal velocity then varies as $r^{-1}$, and the number of particles per unit volume as $r^{-2}$, so the thermal coagulation rate decreases as $r^{-1}$. For fractal dimension of 2, $t_s$ is independent of the size ($r\rho_s$ is constant), so it seems that particles would coagulate into ever-more-diaphanous cobwebs, and never become compact enough to decouple from the turbulence. However, in the regime of small Stokes numbers, other subtle effects contribute to particle collisions. The gas velocity within the smallest eddies changes on the turnover timescale, subjecting it to accelerations of magnitude $\dot{V}_\eta = V(\eta)\Omega(\eta) \sim V(\eta)\Omega_K Re^{1/2} \sim 10^{-2}$ cm s$^{-2}$ (*Weidenschilling*, 1984). Particles have velocities relative to the gas of magnitude $\dot{V}_\eta t_s$. Because coagulation is stochastic, individual aggregates have a dispersion of fractal dimensions about the mean of about ±10% (*Kempf et al.*, 1999), with corresponding dispersion of $t_s$. This implies relative velocities of order $0.1\ \dot{V}_\eta t_s \sim 10^{-2}$ cm/s; relative velocities due to turbulence exceed thermal velocities for aggregates larger than tens of micrometers [an additional growth mechanism for tiny grains was described by *Saffman and Turner* (1956)]. The characteristic growth time is a few hundred years. Fractal aggregates will become compacted once collisional energies become large enough to rearrange bonds between grains. *Dominik and Tielens* (1997) predicted that the threshold energy for rolling of micrometer-sized quartz spheres is ~$10^{-10}$ erg. Collisional energies would exceed this value for millimeter-sized aggregates with masses ~$10^{-6}$ g containing $10^6$ grains. If the energy threshold is higher by two orders of magnitude (section 3.1), compaction would begin for roughly centimeter-sized aggregates (*Blum and Wurm*,

2000). Thus, there is no problem with the initial growth of aggregates from grains in a turbulent nebula. Indeed, turbulence fosters growth in this size range. In a laminar nebula, growth and compaction would occur on longer timescales, driven by differential settling and radial drift at lower velocities. Once compaction occurs, particles begin to decouple from the turbulence ($St_L \geq 10^{-3}$), and relative velocities increase (Fig. 2), along with collision rates. The particles will continue to grow, unless specific energies of collisions exceed their impact strength.

The impact strength of a primitive aggregate in the solar nebula is uncertain; we have no pristine samples of such material. Theoretical analysis by *Dominik and Tielens* (1997; cf. their Fig. 18) suggests that an aggregate of 100 silicate grains, each $10^{-4}$ cm in size, would be disrupted by an impact of energy ~$10^{-6}$ erg, implying ~$10^{-8}$ erg per bond between grains. For grain mass $10^{-12}$ g, this implies a bonding energy ~$10^4$ erg/g for a chain-like aggregate. A compacted aggregate would have more bonds per grain; also, for purely geometrical reasons, disruption of such an aggregate would involve making and breaking multiple contacts between grains as the impact energy propagated through the aggregate. The experimental results of *Blum* (2000) suggest that the break-up energy per monomer is actually about two orders of magnitude higher than predicted by theory, so impact strengths of ~$10^6$ erg/g seem reasonable. The actual values will depend on grain sizes and compositions; any additional bonding besides van der Waals forces (e.g., sintering, chemical reactions, or electrostatic forces) would increase the strength. For example, *Sirono and Greenberg* (2000) used the results described above to estimate the strengths of aggregates. In their model, strengths have complex dependence on grain size and porosity; for our purposes it suffices to note that for monomer sizes of a few tenths of a micrometer, and porosities less than 70%, tensile and compressive strengths are in the ranges ~$10^5$–$10^7$ and $10^6$–$10^8$ dyn cm$^{-2}$, respectively. These values may be compared with the (smaller) measured tensile strengths of one powder by *Blum and Schräpler* (2004) and the (larger) experimentally determined strengths of small, but cohesive, silicate objects (*Love and Ahrens*, 1996, their Fig. 7).

### 3.3. Larger Particles: Settling Toward the Midplane

As particles grow, they acquire larger differential velocities whether or not the nebula is turbulent (section 3.2). Growth accelerates and the packing density of accreted material increases (*Dominik and Tielens*, 1997). Larger particles increasingly decouple from the gas and settle toward the midplane, where their volume density can become much larger than the gas. In this section we describe how the vertical thickness of midplane particle layers is determined, and how this in turn affects accretion.

*3.3.1. Thickness of "the midplane": Role of turbulence.* The intensity of nebula turbulence determines the degree to which particles settle toward the midplane. Even while particles continue to settle, turbulent diffusion produces a mass flux upward, away from the dense midplane. A steady state occurs when these two mass fluxes balance (*Cuzzi et al.*, 1993, equation (52))

$$\rho_p V_z = \mathcal{D}_p \rho_g \frac{d}{dz}\left(\frac{\rho_p}{\rho_g}\right) \approx \mathcal{D}_p \frac{d\rho_p}{dz} = \frac{\mathcal{D}}{1 + St}\frac{d\rho_p}{dz} \qquad (4)$$

where $\mathcal{D}_p$ is the particle diffusion coefficient (section 2.4.2) and the two last expressions assume a constant gas density $\rho_g$, satisfactory for $z < H$. The situation can be greatly simplified by assuming that the local vertical particle velocity $V_z$ is merely the local terminal velocity $g_z t_s = \Omega_K^2 z t_s$ (*Dubrulle et al.*, 1995) (see also section 2.4). This is not always valid (*Cuzzi et al.*, 1993), but it is a fairly good approximation for particles smaller than a meter or so in size in the 2–3 AU region. *Dubrulle et al.* (1995) derived analytical solutions for the thickness of a layer of particles with different radii and densities, and several nebula $\alpha$ values.

The essence of the results can be understood using dimensional scaling of the derivatives in equation (4): Taking $\rho_{po}$ to be some average density near the midplane and $h_p$ the vertical half-thickness of the particle layer

$$\rho_p V_z \approx \rho_{po} \Omega_K^2 h_p t_s = \frac{\mathcal{D}}{1 + St}\frac{\rho_{po}}{h_p} \qquad (5)$$

Giving

$$h_p^2 = \frac{\mathcal{D}}{\Omega_K St(1 + St)} \qquad (6)$$

For global turbulence, $\mathcal{D} = \alpha c H = \alpha H^2 \Omega_K$, thus

$$\left(\frac{h_p}{H}\right)^2 = \frac{\alpha}{St(1 + St)} \qquad (7)$$

Equation (7) shows that the results of *Dubrulle et al.* (1995), which include other terms extending their validity to the $St \rightarrow 0$ limit, can be generalized in terms of a single nondimensional parameter $\mathcal{S} = St/\alpha$ in the limit $St < 1$ (*Cuzzi et al.*, 1996; their Fig. 1). Settling occurs for $\mathcal{S} > 1$; as $\mathcal{S}$ increases, either due to larger particles or weaker turbulence, particles settle into thinner layers.

There is a limit as to how thin a layer can be even if global nebula turbulence is zero, which is set by the influence of the layer itself on the gas. As particle mass density $\rho_p$ reaches and exceeds the gas density, the orbiting particles force the entrained gas to rotate at more nearly Keplerian velocity. Because the gas above this dense layer has no such forcing, it orbits at its slower, pressure-supported

velocity (section 2.4.1). The associated vertical gradient in gas velocity can be unstable to turbulence, which diffuses the particle layer vertically until it reaches a steady state under its own self-generated turbulence (*Weidenschilling,* 1980). Extensive numerical calculations of this effect have been done by *Cuzzi et al.* (1993), *Champney et al.* (1995) (who studied multiple particle sizes), and *Dobrovolskis et al.* (1999). *Dobrovolskis et al.* (1999) improved on the original work of *Cuzzi et al*. (1993) in several important ways, revising a key parameter, and including a new detailed model for damping of local turbulence *by* the entrained particles; the end results of these changes were particle layer thicknesses fairly similar to those found by *Cuzzi et al.* (1993). One can express the effective gas diffusivity within the near-midplane, self-generated turbulence (cf. *Dobrovolskis et al.,* 1999, equation (12); *Cuzzi et al.,* 1993, equation (21)) as

$$\mathcal{D} \approx \frac{(\beta V_K)^2}{\Omega_K \mathrm{Ro}^2} \qquad (8)$$

where Ro is the Rossby number of the turbulent layer, defined such that the largest eddies in the self-generated turbulence have frequency $\Omega_e = \mathrm{Ro}\Omega_K$. To order unity, Ro = Re∗, where Re∗ is the so-called critical Reynolds number that characterizes the relationship of velocity shear to turbulent intensity for a given flow. The constant Re∗ is derived from measured properties of flows in different regimes. Going back to the basic fluid dynamics literature (e.g., *Wilcox,* 1998, Chapter 5 and references therein), *Dobrovolskis et al.* (1999) found that for flows with geometry most similar to that of the nebula midplane, Re∗ ≈ 20–30 rather than the higher values used previously by others. The range of constants seen in various flows introduces perhaps a factor of 2 uncertainty into Re∗.

Using equation (8) for $\mathcal{D}$, and recalling that β can also be written as $c^2/V_K^2$, we obtain

$$\left(\frac{h_p}{H}\right)^2 = \frac{(\beta/\mathrm{Ro})}{\mathrm{StRo}(1 + \mathrm{StRo})} \qquad (9)$$

For particles small enough that StRo < 1, comparing equations (7) and (9) shows that the presence of the layer alone can be identified with a local turbulence equivalent to a global value of $\alpha = \beta/\mathrm{Ro}^2 \approx \beta/\mathrm{Re}*^2 \approx 10^{-6}$. That is to say, global turbulence must be less than this level for the globally laminar solutions (*Cuzzi et al.,* 1993; *Dobrovolskis et al.,* 1999), which are the regime assumed by all midplane particle layer instabilities, to be valid. For larger particles (StRo > 1), the assumptions going into this simple estimate become invalid. In such particle-laden layers, relative velocities between particles all diminish by a factor on the order of $\rho_p/\rho_g$ (*Dominik et al.,* 2006), making incremental growth very plausible.

As pointed out by *Sekiya* (1998) and *Youdin and Shu* (2002), for sufficiently small particles (the one-phase-fluid regime), a different physics takes over. The steady-state layer described by the physics of equation (4) becomes sufficiently extended that its combination of vertical velocity and density gradients stabilizes it against the Kelvin-Helmholz shear instability, which is responsible for generating gas turbulence, so turbulence ceases (section 3.3.3). In this regime, the thickness of this layer is independent of particle size and is given by $h_p/H = \mathrm{Ri}_c^{1/2}H/r$, where $\mathrm{Ri}_c$ = 1/4 is the critical Richardson number (*Sekiya,* 1998). In this limit, $h_p > L_E$ and $\mathrm{Ro} = \Delta V/(\Omega \max(h_p, L_E)) \sim 1$. Decreasing St further will not lead to thicker layers. Setting the small-St limit of equation (9) equal to the critical-Ri thickness above defines the critical Stokes number for which equation (9) loses validity: $\mathrm{St} < 10^{-2}$. Thus the regime studied by *Sekiya* (1998) and *Youdin and Shu* (2002), where for millimeter-radius particles at 2 AU St ~ $10^{-3}$, falls in the Ri-dominated regime. In the outer solar nebula where gas densities are lower, only correspondingly smaller particles will behave this way.

The simple global turbulence model of equation (7) retains its validity for all St. Taking the entire MMN solid density ~$10^{-2}\sigma_g(R)$ in particles of a single size, we can estimate the maximum level of turbulence that would allow unit density particles of a given size to settle into a layer where $\rho_p > \rho_g$ and collective effects become important: $h_p/H < 10^{-2}$. For meter-radius particles, with St ~ 1, $\alpha < 2(h_p/H)^2 = 2 \times 10^{-4}$. For millimeter-radius particles, with St ~$10^{-3}$, $\alpha < 10^{-3}(h_p/H)^2 \sim 10^{-7}$. We return to arguments of this sort in section 3.3.3.

*3.3.2. Timescales for growth and loss by incremental accretion.* In this section we make crude estimates of particle growth and removal rates. We assume the mass growth rate of a particle $\dot{m}$ is dominated by sweep-up of smaller particles, which indeed dominates for all but the very smallest particles. This is a good approximation if velocities are dominated by systematic drift, which is the case if turbulence is low enough to allow settling into a midplane layer. Although larger bodies may dominate the mass distribution, their relative velocities are lower, reducing the collision rate (see *Weidenschilling,* 1988a, 1997, and section 3.2). Then

$$\dot{m} = \pi r^2 \int_0^r V_{rel}(r,r')\rho_p(r')dr' \sim \pi r^2 \overline{V_{rel}(r)}\rho_p(<r) \qquad (10)$$

where $V_{rel}(r,r')$ is the relative velocity between particles of radii r and r', $\overline{V_{rel}(r)}$ is its weighted average over r', and $\rho_p(<r)$ is the particle density in sizes smaller than r. Then the e-folding growth time for mass m is crudely

$$\frac{m}{\dot{m}} = \frac{4\rho_s r}{3\overline{V_{rel}(r)}\rho_p(<r)} \qquad (11)$$

Since both $\overline{V_{rel}(r)}$ and, to a lesser degree, $\rho_p(<r)$ increase with r, the growth time is only weakly dependent on r, plausibly leading to a particle size distribution that evolves in a self-similar way with equal mass per radius bin as seen in

numerical models (*Weidenschilling*, 1997, 2000). Oversimplifying the above expression further by ignoring fractions of order unity, we estimate the growth times in a nebula with average solid particle density $\rho_p$ as

$$\frac{m}{\dot{m}} \sim \frac{\rho_s r}{\overline{V_{rel}(r)}\rho_p} \sim \frac{(100\text{ cm})\rho_s(r/1\text{m})}{\rho_p \beta V_K (r/1\text{m})} \sim \frac{(10^4\text{ cm})\rho_s}{\rho_g \beta V_K \xi}\left(\frac{\alpha}{St}\right)^{1/2} \sim \frac{10^3}{\xi}\left(\frac{\alpha}{St}\right)^{1/2}\text{ yr} \quad (12)$$

where $\xi$ is a sticking coefficient. We took $\overline{V_{rel}(r)} \sim \beta V_K$ for meter-sized particles (section 2.4.1) and used equation (7) to get $\rho_p \sim 10^{-2}\rho_g(H/h_p) \sim 10^{-2}\rho_g(St/\alpha)^{1/2}$. If nebula turbulence is lower, denser midplane layers can form in which particles grow much faster (see below).

One can imagine two removal mechanisms for meter-sized particles: They can drift radially inward at the typical rate of 1 AU/century (but will largely be replaced by other particles drifting from further out), or they can collide with comparable-sized particles and be destroyed. We will return to the fate of drifting particles in section 5. Collisional disruption is primarily a worry in turbulent regimes. In turbulence, meter-sized particles, with St ~ 1, couple to the largest, highest velocity turbulent eddies and acquire random velocities relative to each other on the order of $V_{pp} \sim V_g \sim c\alpha^{1/2} \sim 10$ m/s for $\alpha = 10^{-4}$. As shown in Fig. 2, collisional velocities $V_{pp}$ for both smaller and larger particles are slower. Collision times for meter-sized particles with number density $n_L$ and fraction $f_L$ of total solid mass are estimated as

$$t_{coll} \sim \frac{1}{n_L \pi r^2 V_{rel}} \sim \frac{100\rho_s r}{f_L c \rho_g} \sim \frac{30}{f_L}\text{ yr} \quad (13)$$

where we used equation (7), $n_L = f_L\rho_p/4\rho_s r^3$, and $V_{rel} \sim V_g \sim c\alpha^{1/2}$. Note that $t_{coll}$ is independent of $\alpha$.

Recreating a similar calculation by *Weidenschilling* (1988a), we estimate the radius of the largest particle that can survive such collisions as follows: We require $V_{pp}^2 = StV_g^2 = t_s\Omega_K V_g^2 < E_{crit}/\rho_s$, where $E_{crit} \sim 10^6$ erg cm$^{-3}$ is a plausible strength for a somewhat compacted, meter-sized rubble particle with unit density (section 3.2). The drag regime transitions from Epstein to Stokes for particle sizes in the range of interest. For Epstein drag, we find

$$r < \frac{E_{crit}\rho_g}{\alpha c \rho_s^2 \Omega} \sim \frac{1}{10\alpha}\text{ cm} \quad (14)$$

under nominal asteroid belt conditions ($\rho_g = 10^{-10}$ g cm$^{-3}$, c =$10^5$ cm/s, and $\Omega_K = 5 \times 10^{-8}$ s$^{-1}$). Thus particles of this plausible strength grow to meter radius for $\alpha < 10^{-3}$. However, for this size, the Stokes expression is more relevant, which leads to (see section 2.2)

$$r < \left(\frac{2E_{crit}\rho_g\lambda}{\alpha c \rho_s^2 \Omega}\right)^{1/2} \sim \left(\frac{2}{\alpha}\right)^{1/2}\text{ cm} \quad (15)$$

where we took $\lambda = 50$ cm as the gas mean free path. Here, meter-radius particles survive $\alpha \sim 2 \times 10^{-4}$. Useful expressions that bridge the transition between Epstein and Stokes drag are given by *Supulver and Lin* (2000) and *Haghighipour and Boss* (2003a).

For $\alpha \sim 10^{-4}$, the growth and collisional disruption times are comparable for meter-sized particles, and the drift distance is less than a few AU. Clearly the local population of meter-sized particles is some mix of material originating at a range of locations. Since particle growth times decrease weakly with r (equation (12)), and removal times are more strongly dependent on r, with drift removal and collision velocity approaching maxima at about 1 m radius, one suspects that growth proceeds readily to meter-sized particles, but further growth is frustrated.

This logic suggests that a balance between turbulence and impact strength might allow bodies to approach meter size, but not to exceed that threshold. As velocities induced by turbulence decrease for larger bodies (St > 1), it might seem that once this threshold is passed there is no further obstacle to growth. However, at low levels of turbulence, or even in a laminar nebula, growth may be limited by erosion due to impacts of small particles upon large bodies. The relative velocity between a small particle coupled to the gas and large body moving at Keplerian velocity is $\beta V_K \approx$ tens of meters per second. Cratering experiments with regolith targets (*Hartmann*, 1985; *Weidenschilling*, 1988b) indicate that a transition from net accretion (i.e., ejecta mass less than the impactor mass) occurs at velocities ≤10 m s$^{-1}$, with net erosion at higher velocities. *Wurm et al.* (2001) suggested that gas drag would cause ejecta to reimpact the target, but *Sekiya and Takeda* (2003) showed that they would be swept away by the flow. A target body may experience a range of impacts with gains and losses, with the net effect on its mass dependent on the size distribution of the impactors.

When relative velocities are due to differential drift, impact velocities of small particles onto large bodies approach a constant value of $\beta V_K$, regardless of size. If impacts at this speed are erosive, there may be no threshold size beyond which further growth is assured, as the large bodies would be subject to continued "sandblasting" by small impactors. For accretion to overcome erosion, it may be necessary for impact velocities to decrease. As $\beta$ is proportional to the gas temperature, collisional growth may be delayed as the nebula cools. Another possibility is that the effective value of $\beta$ in the midplane may be decreased by particle mass loading. If particles can settle into a layer with $\rho_p > \rho_g$, then the particles drag the gas within the layer, and its rotation becomes more nearly Keplerian. The effect of such mass loading was analyzed by *Nakagawa et al.* (1986) and included in the coagulation model of *Weidenschilling* (1997), who showed that it could decrease collision veloci-

ties to a maximum of ~10 m $s^{-1}$. Attaining a midplane density sufficient to affect the layer's rotation depends on the particle size distribution (cf. equation (9ff)), but probably requires $\alpha < 10^{-6}$ to ensure easy growth of meter-sized particles without disruption. Thus, it is plausible that a gradually decreasing level of turbulence may lead to a rather abrupt transition from small submeter-sized bodies to large planetesimals.

*3.3.3. Midplane instabilities to breach the meter-sized barrier?* A number of midplane collective effects and instabilities have been pointed out over the years, with the goal of helping primary accretion proceed to and beyond the perceived meter-sized barrier. All these require particle densities well in excess of the gas density, and sometimes far in excess of it, which places rather strict limits on the level of global turbulence. Below we discuss these ideas.

*Particle layer gravitational instabilities:* There are two distinct regimes in which midplane gravitational instabilities have been studied. The first is two-phase models in which the particles are treated as moderately decoupled from the gas, while responding to gas drag, and the gas as having constant density (*Safronov,* 1969; *Goldreich and Ward,* 1973, hereafter *GW73*; *Weidenschilling,* 1980, 1984, 1995; *Cuzzi et al.,* 1993, 1994; *Dobrovolskis et al.,* 1999; *Ward,* 2000). The second is one-phase models in which the particles are so small and firmly coupled to the gas that together they comprise a single fluid with vertically varying density (*Sekiya,* 1998; *Sekiya and Ishitsu,* 2000, 2001; *Youdin and Shu,* 2002; *Ishitsu and Sekiya,* 2002, 2003; *Youdin and Chiang,* 2004; *Yamoto and Sekiya,* 2004; *Garaud and Lin,* 2004). In both cases conditions are sought under which the particle density can become so large that the layer undergoes a gravitational instability.

The original two-phase formulation (*GW73*) was attractive because it suggested that planetesimal-sized objects could be formed directly from centimeter-sized particles in a very thin particle layer, surrounded by a turbulent boundary layer. As discussed in section 3.3.1 (see equation (7)), $\alpha \ll 10^{-6}$ for this scenario to be considered at all. Moreover, *Weidenschilling* (1980) showed that centimeter-sized particles were prevented from settling into a sufficiently thin layer by this very self-generated turbulence, and *Cuzzi et al.* (1993) and *Dobrovolskis et al.* (1999) showed that this conclusion remained true even up to meter-sized particles. Moreover, for particles large enough and velocities small enough to approach the particle density threshold normally cited for instability, only transient gravitational clumps result [like the "wakes" in Saturn's rings (*Salo,* 1992)], and not direct collapse to planetesimals as usually envisioned (*Cuzzi et al.,* 1994). *Tanga et al.* (2004) follow large particles (St $\gg$ 1) in regimes of nominal (marginal) gravitational instability and reproduce just this expected behavior. They then apply an *ad hoc* damping of relative velocities, treated as gas drag acting on much smaller particles with St = 1; this damping allows bound clumps to form that merge with each other over time. However, this study assumed single-sized particles, and *Weidenschilling* (1995) showed that even differential drift velocities in a realistic size distribution would stir the layer too much for it to become unstable. Essentially, by the time particles have formed that are sufficiently large to reach interestingly high midplane densities, the premises of the original instability scenario are no longer valid [see also *Ward* (2000) for a simi-lar conclusion, with caveats about model parameters]. This objection would also apply in the outer solar system where *Möhlmann* (1996) has noted that gravitational instability is more favored. Conceivably, a two-phase gravitational instability might be allowed if the surface mass density of 1–10-cm particles could somehow greatly exceed the nominal solar abundance. Some suggestions have been made along these lines, as discussed below and in section 5. Further studies along the lines of *Tanga et al.* (2004) would be of interest, in which particles of different sizes, with the appropriate St values, were treated self-consistently. Recall that these studies, as with all other midplane instability models, assume a nonturbulent nebula.

The one-phase approach mentioned above (*Sekiya,* 1998, et seq.) assumes particles so small that they cannot separate from the fluid on dynamical timescales. They can, however, settle very slowly into a moderately dense layer *if the global turbulence allows it* (see section 3.3.1 and below). In this regime, the entire (gas plus particle) medium has a strong vertical density gradient that can stabilize the medium against turbulence (the so-called Richardson number criterion). That is, a fluid parcel attempting to become turbulent and rise must work against its natural lack of buoyancy. It turns out that under nominal nebula solid/gas ratios of about $10^{-2}$, the layer cannot become gravitationally unstable in this way. However, it was noted by *Sekiya* (1998), and more emphatically by *Youdin and Shu* (2002), that if the solid/gas ratio were significantly enhanced (factor of 10 or so), a thin layer very near the midplane could become unstable. This is essentially because in such dense layers, the mixed-fluid vertical velocity profile is nearly flat for a considerable vertical range, independent of density — it is saturated, as it were, so unstable shear does not develop. *Gomez and Ostriker* (2005) have found that a more careful treatment of vertical shear leads to a layer that is more prone to turbulence — thicker and less dense by about an order of magnitude — than found by *Sekiya* (1998) and *Youdin and Shu* (2002).

Whether true gravitational instability can can occur via this scenario is problematic. First, particles small enough to satisfy the one-phase approach must have $t_s < (dv/dz)^{-1}$ in the marginally stable layer. The layer must have $h_p/H < 10^{-3}$ to approach gravitational instability ($\rho_p > 10^2 \rho_g$), even if the solid/gas ratio were *enhanced* by an order of magnitude over solar. The shear in this layer, which determines the frequency of nascent eddies, is approximately $\Omega_e \sim \Delta V/h_p \sim 10^3\, \Delta V/H \sim 10^3\, \beta V_K/H \sim 2\Omega_K(R/H) \sim 40\, \Omega_K$. For the one-phase nature, and stabilization by stratification, to be preserved at the onset of instability, $t_s\Omega_e \ll 1$ or St < $10^{-2}$ is thus required. From equation (7) we see this requires the global $\alpha < 10^{-8}$ for the enhanced solids scenario (or $10^{-10}$

for a nominal solid/gas ratio). Second, for such weak nebula turbulence it is hard to imagine particles settling all the way to the midplane without growing at all [see section 3 and *Dullemond and Dominik* (2005)]. Any significant growth would produce self-generated turbulence that would stir the layer (e.g., *Cuzzi et al.*, 1993; *Dobrovolskis et al.*, 1999). Third, mechanisms for enhancing the particle/gas abundance for precisely those particles that are most firmly coupled to the gas are not easily found. *Weidenschilling* (2003a) and *Youdin and Chiang* (2004) get different results regarding the role radial drift might play in enhancing solids (see also below). Achieving this goal by removing gas (by, e.g., photoionization or a disk wind) increases $t_s$, making it harder to satisfy the requirement that $t_s < (dv/dz)^{-1}$ for density stabilization to apply.

Perhaps most difficult of all for the one-phase gravitational instability scenario is a basic physical obstacle that was pointed out by *Sekiya* (1983) but has apparently been overlooked by subsequent workers except for *Safronov* (1991). In a system where the particles are firmly trapped to the gas ($t_s \ll$ the dynamical collapse time $\sim (G\rho_p)^{-1/2}$), gas pressure precludes gravitational instability, in the traditional sense of inexorable collapse on a dynamical timescale, until the solid/gas mass ratio exceeds $10^7$ (at 2.5 AU)! This is 3 orders of magnitude larger than the typically cited thresholds for gravitational instability, and a rather unlikely enhancement. Recent numerical simulations and analytical models support this result (K. Shariff, personal communication and in preparation, 2005). Prior work on midplane instabilities dating back to *Goldreich and Ward* (1973) has treated the "pressure support" term in the dispersion relation as if due to particle random velocities, as decoupled from the gas (as in *Toomre*, 1964), whereas in a one-phase fluid the pressure term involves the far larger gas sound speed, divided by a mass-loading factor. Only for huge loading factors does the gas pressure support term become as small as the traditional pressure support term and allow instabilities to grow (*Sekiya*, 1983). Physically, what happens is that incipient collapse by the mass-dominant particles compresses the entrained gas, leading to an outward pressure gradient that forestalls further collapse of the gas (and trapped particles).

*Sekiya* (1983) suggests that an *incompressible* three-dimensional mode can emerge for solid/gas mass-loading ratios comparable to the so-called "Roche density" ($\rho_R \sim 15(3\,M_\odot/4\pi r^3) \sim 10^3\,\rho_g$). The nature of these modes has never been followed, and the fate of solid material within them would seem to be less in the nature of an instability than merely further settling at, effectively, slow terminal velocity. Of course, achieving even the Roche density in a midplane environment still faces the obstacles mentioned above (see section 4, however).

*Can enhancement of particle surface density by global radial drift foster gravitational instability?* In section 5 we describe how radial drift might lead to significant changes in the local density of solids relative to nominal solar abundance. One naturally asks whether this effect might play a role in fostering instabilities. *Stepinski and Valageas* (1997) and *Kornet et al.* (2001) noted large enhancements in the surface mass density of solids in a range of sizes, due to this effect. Of course, the nebula must still be globally nonturbulent, and one still has to deal with the distinction between transient wavelike instabilities and direct collapse to planetesimals (*Cuzzi et al.*, 1994). Application of radial drift enhancement to the one-phase instability (*Youdin and Shu*, 2002; *Youdin and Chiang*, 2004), besides facing the serious obstacle of gas pressure mentioned above, requires millimeter-sized particles to drift many AU, over $10^5$–$10^6$ yr, in a dense midplane layer with low relative velocities, without growing at all. This process depletes the outer nebula of solids while enhancing the inner region; numerical models (*Youdin and Shu*, 2002; *Youdin and Chiang*, 2004) achieve the critical density inside a few AU, but effectively denude the nebula of solids at larger distances. This migration would have to occur before the formation of the outer planets, which would otherwise act as barriers to drift. In that case, no material would be left from which to make their cores, or comets (*Weidenschilling*, 2003a). Also, the extent of drift would mean that much of the material that formed the terrestrial planets and asteroids originated at much larger heliocentric distances; the implications for the chemistry of this matter has not been addressed.

*Can enhancement of large particles inside nebula vortices or spiral density waves foster gravitational instability?* It was pointed out by *Barge and Sommeria* (1995), and studied further by *Tanga et al.* (1996), *Bracco et al.* (1998), and *Klahr and Bodenheimer* (2003b), that large, two-dimensional, circulating vortices (*not* true turbulent, randomly fluctuating eddies) had the ability to concentrate meter-sized boulders near their centers. This is a specific form of fostering gravitational instability by increasing surface mass density. Comparable effects related to spiral density waves (in a globally gravitationally unstable nebula) were mentioned in section 2.4.1.

Long-lived vortices rotate clockwise, in the sense of the local radial gradient. Meter-sized boulders are most affected because their $t_s$ is comparable to the rotation time of these vortices. In the enhanced headwind of these vortices ($\sim\beta^{1/2}V_K$ rather than $\beta V_K$), meter-sized boulders drift radially by about the extent of a scale-height-size eddy in one orbital period. When in the outer part of the vortex, meter-sized particles suffer a stronger than normal headwind and their semimajor axis shrinks. When on the inner part, they incur a comparably strong tailwind and their semimajor axis expands. In the local co-rotating frame, they appear to spiral in to the center of the vortex. While some studies indicate vortices of this sort are long-lived (*Godon and Livio*, 2000), other studies indicate they are not (*Davis et al.*, 2000), so it is not clear what the net effect of this concentration might be. Recently *Barranco and Marcus* (2004) have obtained a solution for the full three-dimensional flow in such a large vortex; surprisingly, the rotational flow vanishes near the midplane where meter-sized particles would lie. Furthermore, one must wonder if all the motion

in these giant vortices — with speeds approaching the sound speed — can exist without producing some degree of internal turbulence that would preclude even meter-sized particles from settling to the midplane, so any instability mechanisms would remain precluded. As particles collided and broke into smaller particles, the rubble would escape the vortex. Overall, for several reasons, we think this effect probably does not play a significant role in primary accretion.

In spiral density waves, the compressional effect is systematic and is not thought to add to the random velocity (W. Rice, personal communication, 2005), but preexisting three-dimensional dispersions of material are retained and the wave itself might increase nebula turbulence (*Boley et al.,* 2005). Whether or not the increased abundance (and thus collision rate) leads to increased accretion in either waves or vortices depends on the relative collision velocities. Similar concerns apply to concentrations of boulders found in less systematic radial bands of locally high gas pressure (*Fromang et al.,* 2005; *Johansen et al.,* 2005).

*Secular instability?* A third class of midplane instability model is the drift instability (*Goodman and Pindor,* 2000), which also presumes a globally nonturbulent nebula with quite low $\alpha$ ($\ll 10^{-6}$; section 3.3.1) in order for particles to drive gas velocities. The midplane layer is thought of as a unit drifting inward at a single speed that depends on its surface mass density. As shown by *Nakagawa et al.* (1986), *Cuzzi et al.* (1993), and *Dobrovolskis et al.* (1999), dense particle layers are self-shielded from the gas — they drive the entrained gas closer to the Keplerian velocity, and suffer a much weaker headwind than isolated particles — thus drifting inward more slowly. The premise is that, if some patch of the layer became slightly more dense than its radial neighbors, its drift rate would slow down and material from outside could catch up with it, further increasing its density. This suggestion is interesting, but under perhaps more realistic conditions, where particles in the layer have a range of different sizes and drift rates, as well as particles at different vertical levels in the layer having different drift rates, it would probably be washed out. *Weidenschilling* (2003a) points out that there is a feedback between a local density enhancement and turbulent stress. If a section of the particle layer becomes more dense, then its orbital speed increases, becoming more nearly Keplerian. This increases the shear between the layer and the surrounding gas, and acts to counter the slower drift rate that would result from the density enhancement. This effect depends on the degree of coupling of the particles and the gas, i.e., on their size. It is not taken into account by *Goodman and Pindor* (2000), and its significance is still a matter of controversy. *Safronov* (1991) and *Ward* (1976, 2000) also mention several longer-term, *secular* or *dissipative* instabilities that thin layers are subject to, again if global turbulence is vanishingly small. These are worthy of more study, but the dispersion relations on which these are based are only valid for nonturbulent nebulae, and turbulence will add diffusion terms that will stabilize short lengthscales.

*Summarizing:* Midplane instabilities of various kinds have been suggested as ways to allow growth to continue into and beyond the problematic meter-sized "barrier." However, as described above in section 3, recent incremental growth models find that the growth beyond meter size is not a problem in nonturbulent regimes, and the instability approaches are invalid in even weakly turbulent regimes where the meter-sized barrier may be a problem. Furthermore, long-neglected gas pressure effects make gravitational instability much more difficult for small particles than widely believed. It may be that local, large-scale, gas dynamical structure in the nebula might be able to increase the density of particles, and thus their collision frequency. However, the net result for accretion depends on the specifics of random collision velocities, which have not been modeled in these scenarios.

## 4. TURBULENT CONCENTRATION: FINGERPRINTS IN THE ROCKS

In this section we describe an aerodynamic process that is new since the original volume in this series (*Kerridge and Matthews,* 1988) and has the potential for breaching the meter-sized barrier and producing objects that look like actual meteorite parent bodies. The process is preferential concentration in turbulence, or turbulent concentration.

### 4.1. The Basic Process

One's intuition is that turbulence is a dispersive, homogenizing, and mixing process, and indeed this is true from the standpoint of the global scale trajectories of particles of *all* sizes (i.e., the $V_p$ of section 2.4.2). However, numerical simulations (*Squires and Eaton,* 1990, 1991; *Wang and Maxey,* 1993; *Cuzzi et al.,* 1996, 2001; *Hogan et al.,* 1999) and laboratory experiments (*Eaton and Fessler,* 1994) show that particles having a narrowly selected aerodynamic stopping time $t_s$ actually concentrate in dense zones in turbulent, incompressible fluids. Particles avoid zones of higher vorticity in the gas, so the more densely populated zones are those of lower vorticity. The dense zones move in inertial space, following the fluid properties that foster them. This effect is entirely different in its basic physics, and applies to particles with entirely different properties, than vortex-center concentration of meter-sized boulders as discussed in section 3.3.3. Turbulent concentration is a way to aerodynamically select particles of a very specific $t_s$ for significant local concentration — by orders of magnitude. In the next two subsections we address (1) the size-selection criteria and (2) the concentration factor *C.*

### 4.2. Size Selection and Size Distribution

Preferentially concentrated particles have stopping time $t_s$ equal to the overturn time of the Kolmogorov scale eddy, $t_e(\eta)$ (*Wang and Maxey,* 1993). We will sometimes refer to these particles as having Stokes number $St_\eta = t_s\Omega(\eta) = t_s/$

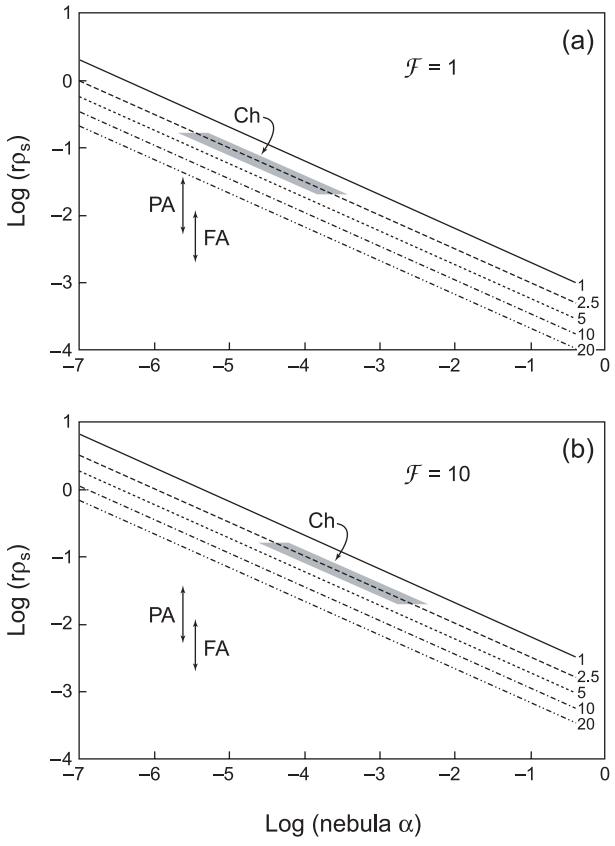


**Fig. 3.** The radius-density product for preferentially concentrated particles in nebula turbulence of different intensity levels α (equation (16)), depicted at several distances (AU from the Sun) in a typical protoplanetary nebula model (*Cuzzi et al.*, 2001) with **(a)** no enhancement ($\mathcal{F}$ = 1) and **(b)** a factor of 10 enhancement ($\mathcal{F}$ = 10) over the total surface density of a MMN. Denser nebulae concentrate the same $r\rho_s$ at higher α. Observed chondrules fall in the vertical range indicated by the shaded area on the line at 2.5 AU. Porous aggregates (PA) and fluffy aggregates (FA) would have lower $r\rho_s$ products, and would be similarly concentrated at lower gas densities.

$t_e(\eta) = 1$. *Cuzzi et al.* (1994, 1996, 2001) showed that this constraint pointed directly to chondrule-sized silicate particles when nominal nebula conditions were assumed. The stopping time $t_s = r\rho_s/c\rho_g$ is easily related to nominal nebula and chondrule properties. We recall from section 2.2 the eddy time $t_e(\eta) = \Omega_K^{-1}Re^{-1/2}$, and $Re = \alpha cH/\nu_m$. These relationships can be easily combined into a very general expression for the preferentially concentrated particle, having radius r and density $\rho_s$

$$r\rho_s = 6.3 \times 10^{-4} \left(\frac{\mathcal{F}}{\alpha}\right)^{1/2} \left(\frac{R}{1\ AU}\right)^{-3/4} \ g\ cm^{-2} \qquad (16)$$

In the above expression, a nebula has been assumed with surface mass density $\sigma(R) = 1700\ \mathcal{F}(R/1AU)^{-3/2}$ g cm$^{-2}$, where $\mathcal{F}$ is the enhancement over a MMN (*Cuzzi et al.*, 2001). Predictions are shown in Fig. 3. Note that a number of combinations of α and nebula density (here represented by distance from the Sun) can concentrate the same particle radius-density product $r\rho_s$. The actual value of nebula α remains very uncertain (section 2.1). Based on nebula lifetimes, and assuming that nebula viscosity is basically the mechanism responsible for disk evolution, values in the $10^{-5}$–$10^{-2}$ range are usually inferred. Note also that smaller particles, and/or particles of much lower density — porous or even "fluffy" aggregates — are also concentrated by this process, but in regions of much lower gas density (or higher α) than for solid chondrules. This might be highly relevant for outer solar system accretion, in regions where, perhaps, nearly solid "chondrule"-like particles do not form; however, it might be hard to find evidence for such an effect.

Not only the typical size, but also the characteristic size distribution of meteorite constituents seems to be in good agreement with the predictions of turbulent concentration. *Paque and Cuzzi* (1997) and *Cuzzi et al.* (2001) compared the typical size and density of chondrules separated from five different carbonaceous and ordinary chondrites with model predictions of relative abundance as a function of particle stopping time (as expressed in terms of $St_\eta$) and aligning the peaks of the theoretical and observed plots to compare the shapes of the curves. The agreement is very good, especially given that the theoretical values have no free or adjustable parameters (*Hogan and Cuzzi*, 2001).

Aerodynamic size sorting subsequent to chondrule formation might not be the whole story, of course; the process(es) by which chondrules, CAIs, and metal grains formed in the first place certainly did not produce an infinitely broad size distribution. Some heating mechanisms, notably shock waves in the nebular gas (see *Connolly et al.*, 2006), might have preferentially melted millimeter-sized objects; tiny chondrule precursors might have evaporated, and very large ones would not be melted thoroughly, if at all. Alternatively, it has been suggested that surface tension in silicate melts played a role in helping determine chondrule size distributions (e.g., *Liffman and Brown*, 1995, and others).

However, as discussed in section 2.2.1, extensive studies of the size distribution of chondrule-sized particles in meteorites, using thin section and disaggregation techniques (*Hughes*, 1978, 1980), have determined that both true, rounded chondrules and broken "clastic fragments" of once-larger chondrules follow the same size distribution. Apparently, some chondrules were formed with sizes much larger than those in the meteorite, but only after being fragmented by some other process at a later time could their fragments be size-sorted into the parent body along with whole chondrules of similar size. Also, *Krot et al.* (1997) report tiny "microchondrules" in accretionary rims around many chondrules in type 3 chondrites; they are especially abundant in some cases. Since the chondrule-formation process seems to have resulted in size distributions broader than those that are typically found in the chondrites, the narrow observed

size distribution probably is not best explained by a process acting only on the liquid state, such as surface tension, or perhaps by the formation process at all. Furthermore, *Cuzzi et al.* (1999) note that the fit of Fig. 4 is considerably improved if individual chondrule radius-density products are used, rather than assuming some average density; this implicates aerodynamics at a stage between formation of chondrules and similar objects, and their accretion. Other approaches to aerodynamic sorting (*Huang et al.,* 1996; *Ackridge and Sears,* 1998) favor a postaccretionary, parent-body process using effluent vapor to create a fluidized bed in which denser particles settle relative to less-dense ones.

An open question that would be valuable to resolve is the detailed size distribution of the irregularly shaped and often porous CAIs, as well as the irregularly shaped metal grains, found in different meteorite types. While the fact that chondrites with large chondrules (CVs) also have large CAIs (type B) and chondrites with small chondrules have small CAIs, it also appears that most type B CAIs are larger than most CV chondrules. Can this be reconciled by density/porosity differences? It is hard to say, as quantitative measurements of CAI size distributions are minimal at best (*May et al.,* 1999).

The agreement of both the characteristic size, and size distribution, of chondrules with the simplest predictions of turbulent concentration theory are what we call fingerprints of the process. A third fingerprint might be present in the relationship of fine-grained accretion rims to their underlying chondrules (section 6.3).

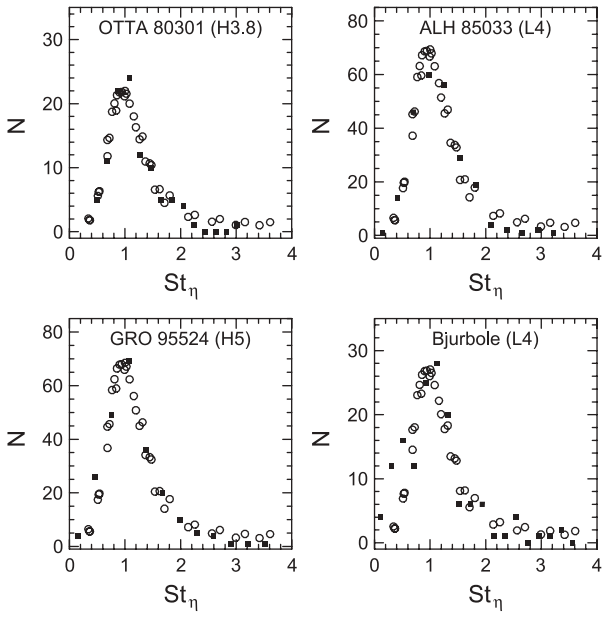


**Fig. 4.** Comparison of observed chondrule size-density distributions $N(r\rho_s)$ from four different meteorites (solid symbols) with theoretical predictions (open symbols) (*Cuzzi et al.,* 2001). The observed distributions are merely assumed to peak at $St_\eta = t_s/t_\eta = 1$ and are aligned with the predictions (which have no free parameters and are the same in all panels).

### 4.3. How Much Concentration?

Particle concentration shares a number of properties with other properties of turbulence that are termed *intermittent*. For instance, it is widely known that dissipation of turbulent kinetic energy ε occurs on the Kolmogorov scale; it is less widely known that the spatial distribution of this quantity is highly nonuniform. While locally and temporally unpredictable and fluctuating widely (i.e., intermittent), ε has well-determined statistical properties — its probability distribution function (PDF) is well determined on any lengthscale. Furthermore, it has been shown that the PDFs of both ε and particle concentration share a fractal-like descriptor called the singularity spectrum that is independent of Reynolds number. Determining this fundamental rule of the process (*Hogan et al.,* 1999, and references therein) allows one to predict the PDFs of both ε and particle concentration at any Re (*Cuzzi et al.,* 2001), as long as the process remains independent of lengthscale. This behavior is closely related to the idea that turbulence is a scale-independent cascade process. That is, transport of kinetic energy, vorticity, and dissipation from their sources at large scales to their sinks at small scales obeys rules that are independent of scale. Scale-independence and Re-independence are connected because Re determines the depth of the inertial range: $Re^{3/4} = L/\eta$ (section 2.2). That is, larger Re means a larger number of eddy bifurcations between L and η, and stronger fluctuations in intermittent properties (see, e.g., *Meneveaux and Sreenivasan,* 1987).

The behavior of both ε and *C* can be explained nicely using a cascade model, where upon bifurcation of a unit volume parent eddy into two equal-volume daughter eddies, some quantity x is partitioned unequally, following some multiplier p. Then the density of x becomes p/0.5 in one subeddy and (1 – p)/0.5 in the other. If $p \neq 0.5$, fluctuations in the density of x emerge that grow with successive levels in the cascade. Cascades can be crudely modeled with constant p; more realistically, p is chosen at each level from a PDF that itself is independent of level in the cascade (*Sreenivasan and Stolovitsky,* 1995b). The PDF of multipliers is the rule that is level, or Re, independent. Excellent agreement has been obtained for high-Re turbulence with models of this sort.

However, changing physics can change the rule. Specifically, increasing local particle concentration and the associated mass loading $\rho_p/\rho_g \gg 1$ can locally kill off the turbulence that leads to intermittency. In new work that is as yet incomplete, cascades are being modeled in which the multiplier PDF can be made conditional on local particle density, to account for the effects of mass loading and turbulence damping. Full three-dimensional simulations are being used to determine how multiplier PDFs depend on $\rho_p/\rho_g$. Preliminary results (R. C. Hogan and J. N. Cuzzi, in

preparation, 2004) indicate that concentration continues to grow well after local particle density significantly exceeds the local gas density: regions of $\rho_p \sim 100\ \rho_g$ are seen with low but interesting probability even at fairly low Re, and with increasing probability at higher nebula Re. The goals of ongoing work include determining the lengthscales on which, and the probability with which, zones of different density occur.

### 4.4. Getting to Planetesimals

In this section we speculate on how, or whether, the fingerprints of turbulent concentration might become directly manifested in actual meteorite parent bodies. Even a particle density in the densest zones is still far from solid density; other physics must come into play to transform dense, particle-rich parcels of the nebula, with mass density less than that of cotton candy, into a meteorite parent body or its immediate precursor. This process remains unstudied and is fraught with obstacles. The scenarios sketched below by which this evolution may proceed are not in any way proven, but intended to provoke further thought and discussion.

Dense, particle-rich zones experience solar gravity as a unit; at lower density than gravitational instability can set in, they begin to settle toward the midplane and move azimuthally through the surrounding gas. The ensuing gas ram pressure and shear flow of displaced gas around the sides of the clump, and perhaps buffeting by turbulent fluctuations it must traverse as it moves, can destroy a strengthless clump in the absense of a counteracting force. However, counteracting forces might exist. Analogies can be sought in the behavior of fluid drops settling in lower density fluids. Pressure stresses quickly destroy fully miscible drops, but surface tension allows strengthless drops to survive and settle as units (*Thompson and Newhall,* 1885; *Clift et al.,* 1978; *Frohn and Roth,* 2000). In the nebula context, the self-gravity of the dense clumps might play a role analogous to surface tension. To the extent that turbulent concentration can produce sufficiently dense regions before viscous disruption occurs, self-gravity might be able to sustain these entities as they settle toward the midplane, or coagulate with similar dense clumps. Once densities and collision rates became high enough, collective electrostatic (dipole-dipole) forces, due to tribocharging in dense clusters (section 3.1), might also increase the binding energy of clumps that were still far from solid.

Candidate dense zones must be considerably larger than the Kolmogorov scale $\eta$. The dynamical time of a clump with the Roche density $10^3$–$10^4\ \rho_g$ (section 3.3.3) is $t_{coll} \sim (G\rho_p)^{-1/2}$, roughly a few weeks. In order for this material to survive being torn apart by eddy motions, it must be larger than eddies with this timescale. Since eddy times scale as $\ell^{2/3}$ (section 2.2), and the Kolmogorov scale eddy $\eta \sim 1$ km has an eddy time of several thousand seconds, stably bound zones with $\rho_p \sim 10^3$–$10^4\ \rho_g$ must also be of a size scale $\geq 100\ \eta$. The abundance of very dense zones, at fairly large scales, remains to be determined (section 4.3). If spiral density waves repeatedly pass through the nebula, condensing gas and embedded particles by an order of magnitude or more as they pass (e.g., *Rice et al.,* 2004), achieving critical density for gravitational instability might become easier. Clumps with these properties have masses greatly exceeding the "meter-sized barrier," and might be the direct precursors of large planetesimals composed entirely of similarly-sized objects ("chondrules" and their like).

Certainly, these scenarios for the terminal stage of primary accretion remain only suggestive and are untested. We return to the issue of primary accretion in section 6.4, after discussing one more process with important implications for planetesimal formation and meteorite properties — radial decoupling of planetesimal-forming materials from the nebula gas.

## 5. RADIAL MIXING: DECOUPLING OF PLANETARY MATERIALS FROM THE GAS

Aerodynamic effects can lead to significant radial redistribution of material. These motions are of several possible types. As mentioned in section 2.4.1, large particles generally incur a headwind and drift rapidly inward. In the presence of turbulence, particles in the chondrule-CAI size range and smaller are coupled to gas motions quite well, and their random velocities $V_p$ induce radial and vertical diffusion much like that of gas molecules. While hydrogen molecules are all the same, small solid particles retain a memory of the chemistry, mineralogy, petrology, isotopic content, and crystallinity of their formation region. Diffusion in the presence of radial gradients in any of these properties can lead to significant, and potentially observable, radial evolution of small particles — both inward and outward. Also, direct outward radial transport by stellar or disk winds well above the disk can also be significant for small particles, primarily in the early stages of disk evolution when they are most vigorous.

In this section, we discuss outward ejection of small particles by winds, and inward drifts due to gas drag (especially in connection with evaporation boundary transitions). We discuss diffusion in section 6.

### 5.1. Outward Ejection by Stellar and Disk Winds

Some theories (see *Connolly et al.,* 2006; *Chaussidon and Gounelle,* 2006) posit formation of CAIs and/or chondrules very close to the protosun (several protostellar radii; about 15 $R_\odot$, or less than 0.1 AU), not far from where nebula gas funnels into the star along magnetic field lines. In these theories, outward transport to parent-body formation regions near 2–3 AU is attributed to entrainment in the stellar wind (*Skinner,* 1990a,b; *Liffman and Brown,* 1995;

*Shu et al.*, 1996, 1997). *Shu et al.* (1996) define a parameter that we simplify slightly and call $\zeta$

$$\zeta = \frac{3\dot{M}_w}{16\pi R_x^2 \Omega_x \rho_s r} \quad (17)$$

where $\dot{M}_w$ is the total mass flux in the stellar wind, and $R_x$ and $\Omega_x$ are the radius and rotation frequency at the x-point near 15 $R_\odot$, from where the stellar wind originates in this theory. For simplicity we have used $\Omega_x$ rather than the comparable rotation frequency of the star itself, and dropped a constant of order unity. The density of the emerging wind at the launch site is

$$\rho_x \sim \frac{\dot{M}_w}{4\pi R_x^2 V_w} \sim \frac{\dot{M}_w}{4\pi R_x^3 \Omega_x} \quad (18)$$

and so the coupling parameter $\zeta$ can be seen to be

$$\zeta = \frac{3}{4}\frac{\dot{M}_w}{4\pi R_x^3 \Omega_x}\frac{R_x}{r\rho_s} \sim \frac{c\rho_x}{r\rho_s}\frac{R_x}{c} = \frac{R_x/c}{t_s} = \frac{R_x/H}{\Omega_x t_s} \quad (19)$$

For present purposes we can ignore the difference between the wind speed and the sound speed c, so $\zeta$ can be regarded as the ratio of the time for the wind to travel out of the region to a particle stopping time. For the very hot plasma at the x-point, $R_x/H \sim 0.3$, so $\zeta \sim 0.3/St_x$ where $St_x = t_s\Omega_x$, a Stokes number with $\Omega_x$ serving as the normalizing frequency.

A similar derivation for the ratio of the gravitational force on a particle to the gas drag force on it ($\pi r^2 \rho_x V_x c$) reveals them to be equal when $St_x = 1$. Particles experiencing a drag force comparable to gravity, even if it begins in the tangential direction, have their orbits severely perturbed and are slung outward, as well as being lifted out of the plane by the wind. *Shu et al.* (1996) find that, to reach the several-AU region, particles with $St_x \sim 1$ are required. A similar derivation by *Liffman and Brown* (1995; their equation 3.9) gets a similar result.

*Shu et al.* (1996) found that the throw distance is fairly sensitive to $\zeta$, and suggested that the wind could thereby play a role in size-sorting of chondrules and/or CAIs. However, a more recent version of the x-wind model (*Shu et al.*, 1997) proposes radial fluctuations in the launching point, on decadal timescales, caused by magnetic flux variations in the x-region (typically <0.1 AU). There are several-orders-of-magnitude changes in gas density across the x-point. The wind density fluctuations experienced by particles at different distances, as the launch point sweeps back and forth across them, would cause wide variations in the launch aerodynamic parameter $\zeta$, calling into question whether this mechanism can, by itself, be responsible for the very narrow chondrule size distributions.

It should also be noted that other theories for the observed stellar winds have them originating over a much wider range of disk radii — up to several AU (so-called "disk winds") (e.g., *Königl and Pudritz*, 2000). Recall from equation (18) above that the entrainment gas density, and thus the drag force, is derived by assuming the entire observed wind mass flux $\dot{M}_w$ arises from a very small region of scale $R_x < 0.1$ AU. Disk winds have a much more extended source and thus a far lower entrainment gas density, and therefore may not be capable of ejecting chondrule- or CAI-sized particles. Some recent papers have provided support for disk winds, at least as causing the lower-velocity winds where most of the mass flow $\dot{M}_w$ appears (*Anderson et al.*, 2003; *Hartmann and Calvet*, 1995). It would be useful to resolve this issue.

### 5.2. Inward Radial Drift of Large Particles and Mass Redistribution

Global scale radial redistribution of large solid particles relative to the gas, under gas drag, was first discussed in detail by *Stepinski and Valageas* (1996, 1997). Since that time it has been studied further by *Kornet et al.* (2001) and *Weidenschilling* (2003a). *Morfill and Völk* (1984) had addressed the problem earlier in general terms, but with a specific application to particles that were too small to show much of a drift-related effect. *Stepinski and Valageas* (1996, 1997) (and *Kornet et al.*, 2001) simplified complex processes into a semi-analytical model to obtain insights into the global parameter space within which solids evolve. Among their simplifications was a single local particle size and collisions driven primarily by turbulence; however, *Weidenschilling* (1997, 2003a) argued that collisional growth is driven primarily by size differences and corresponding systematic velocity differences rather than turbulence (section 3). Nevertheless, some interesting qualitative conclusions emerge. In all these models, outcomes are determined by a race between growth and drift. In general, solids grow and drift fast enough to deplete the outer disk of solids while enhancing the solid/gas ratio further inward. This redistribution in surface mass density is essentially a radial convergence effect associated with the cylindrical geometry and the dependence of drift velocity on location and particle size (cf. section 3.3.3). However, migration stops when (if) coagulation produces bodies large enough (kilometer-sized or larger) for the drift rate to decrease to low values (cf. Fig. 1), and does not necessarily deplete the outer nebula of solids or produce a large enhancement in the inner nebula. Fairly abrupt outer edges are seen in the final radial distribution of solid bodies. *Stepinski and Valgeas* (1997) noted that this might explain the abrupt outer boundary of the Kuiper belt. This edge effect is enhanced in the models of *Weidenschilling* (2003b), which include a distribution of particle sizes. At some distance that depends on the nebular parameters, bodies grow large enough to stop drifting inward; they then effectively capture smaller particles com-

ing from further out, causing mass to pile up at a distance that is typically a few tens of AU.

### 5.3. Enhancement of Solids Outside Condensation/Evaporation Boundaries

Both radially inward drift of solids, and radially outward diffusion of vapor, can lead to enhancements in surface mass density of solids relative to solar abundance. *Morfill and Völk* (1984) and *Stevenson and Lunine* (1988) addressed enhancement of solid surface mass density just outside a condensation/evaporation boundary at $R_{ev}$. Stevenson and Lunine assumed the presence of a *cold finger* — a complete sink of material — just outside the boundary. Then, vapor would be steadily diffused outward towards this sink and the inner solar system dried out. Stevenson and Lunine emphasized water and its possible role in augmenting the surface mass density just outside $R_{ev}(H_2O)$, speeding the formation of Jupiter's core; moreover, this process would work in a similar way for any volatile. *Morfill and Völk* (1984) combined outward diffusion with inward particle drift, but ended up treating only particles that drift only slightly faster than the nebula gas and never developed an efficient sink at $R_{ev}$, so the net effects were not striking by astrophysical standards. *Cuzzi and Zahnle* (2004) show how the buildup of solid material outside evaporation fronts may be dominated by radial inward drift of meter-sized rubble, rather than outward diffusive transport from the inner nebula, and find that order(s) of magnitude effects are possible.

### 5.4. Vapor Enhancement and/or Depletion Inside Evaporation Fronts

In addition to the enhancement of surface mass density in solids just outside of condensation/evaporation boundaries, there is the potential for significant enhancement of vapor abundances of volatile material at radii further inward than solids can exist. *Cyr et al.* (1998, 1999) noted how the complete removal of water from the inner solar system by the *Stevenson and Lunine* (1988) cold finger might lead to problems explaining the oxidation states of many meteorites, and explored how a leaky cold finger might allow, say, meter-sized particles to carry water vapor back into the inner solar system. Unfortunately, these calculations are inconsistent with very similar calculations by *Supulver and Lin* (2000), which show that even meter-sized particles do not survive far inside the evaporation radius. Independent estimates of evaporation and drift rates, by J.N.C. and by F. Ciesla (personal communication, 2003) support the results of *Supulver and Lin* (2000); however, Supulver and Lin do not address vapor abundances inside $R_{ev}$. *Morfill and Völk* (1984) found that the vapor abundance inside $R_{ev}$ was always solar; however, this was partly because their sink at $R_{ev}$ remained quite leaky, and partly because of what seems to be an overly restrictive outer boundary condition (their equation B7).

The variation of vapor abundance inside evaporation fronts has recently been reinvestigated by *Cuzzi et al.* (2003) and *Cuzzi and Zahnle* (2004), who emphasize the role of rapidly drifting large boulders in transferring mass. They find that large enhancements can occur in the vapor phase. Below we sketch the approach as slightly simplified from *Cuzzi and Zahnle* (2004) for some volatile species with local concentration C(R), nominal solar abundance $C_o$, and evaporation boundary at $R_{ev}$. The process is illustrated in Fig. 5.

The equation for the evolution of C in a one-dimensional cartesian form, with no distributed sources or sinks, and all properties held constant except C(R,t), is

$$\frac{\partial}{\partial t}(\sigma_g C(R,t)) + \frac{\partial}{\partial R}(\Phi(R,t)) = 0 \qquad (20)$$

where the radial mass flux $\Phi(R,t)$ is the sum of nebula advection, diffusion, and midplane mass drift respectively

$$\Phi(R) = -C\sigma_g V_n - \mathcal{D}\sigma_g \frac{dC}{dR} - \sigma_L V_L \frac{C}{C_o} \qquad (21)$$

In the last term of $\Phi(R,t)$, $\sigma_L$ is the surface mass density of solids in the meter-sized range away from the boundary; these particles drift rapidly at velocity $V_L$ (section 2.4.1). Their abundance is proportional to the local abundance C close to the boundary. A dimensionless sink term $\mathcal{L}$ (defined below) is introduced at $R_{ev}$, due to accretion onto a band of planetesimals having optical depth $\tau_{PL}$, in a region of width H just outside $R_{ev}$. These can only provide a true sink if they are too large to drift inward past $R_{ev}$ (have radii $r_{PL}$>1 km or so).

Inside the evaporation front ($R < R_{ev}$) the steady-state solution to this simple system is an enhancement factor over cosmic abundance, which can be approximated by

$$\frac{C}{C_o} = \frac{E_o}{1 + \mathcal{L}} \qquad (22)$$

where

$$E_o = 1 + \frac{\sigma_L V_L}{C_o \sigma_g V_n} = 1 + \frac{f_L V_L}{V_n} \qquad (23)$$

and

$$\mathcal{L} \equiv \tau_{PL} \frac{f_L V_L}{V_n \alpha^{1/2}} \qquad (24)$$

In the equations above, $f_L = \sigma_L/C_o\sigma_g$ and for simplicity here is assumed to be $\ll 1$. The planetesimal accretion rate is determined by the large particles lying in a layer of thickness given by equation (17), and perfect sticking is assumed. $E_o$ is easily determined from its component parts

$$E_o \approx \frac{f_L V_L}{V_n} \sim \frac{f_L \beta V_K}{(\alpha c H/R_{ev})} \sim \frac{f_L}{\alpha} \qquad (25)$$

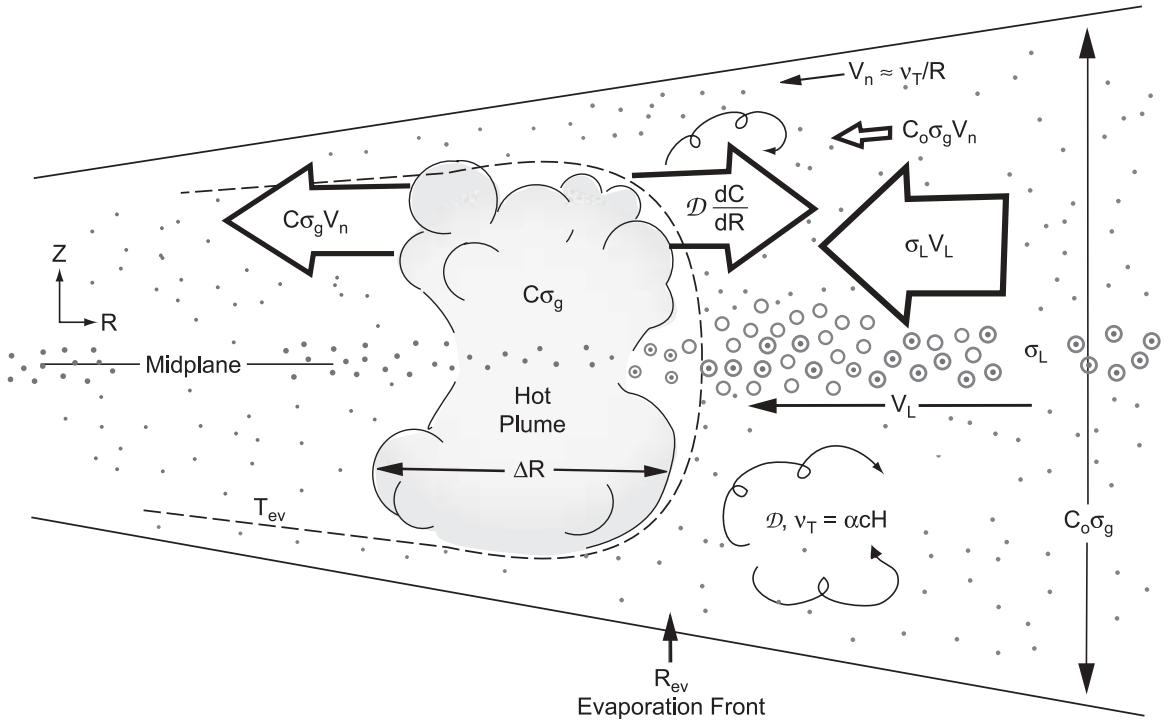


**Fig. 5.** Sketch illustrating inwardly drifting volatile material crossing its evaporation front $R_{ev}$, with midplane temperature $T_{ev}$. The large inward drift flux of midplane solids $\sigma_L V_L$ cannot be offset by vapor removal processes $C\sigma_g V_n + \mathcal{D}\sigma_g dC/dR$ until the concentration of the vapor C is much greater than nominal solar $C_o$. More refractory material, shown here as a minor constituent, simply goes on drifting and growing.

where $V_L \sim \beta V_K$ and $\beta \sim (H/R)^2$ (section 2.4.1), $V_K$ is the Keplerian velocity, and $c = H\Omega$. As discussed in section 3.3.2 (cf. also *Cuzzi et al.*, 2003), size distributions quickly form by incremental growth containing equal mass per decade from micrometers to meters or so, so $f_L \approx 0.1$ is not unreasonable. Then for plausible values of $\alpha$, $E_o \geq 10$–$100$. *Morfill and Völk* (1984) had a parameter analogous to $E_o$ (their $\lambda = V_L/V_n$), but set it to unity, underestimating the power of mass supply by radial drift of large particles. In the limit of very small $\alpha$, collective effects cause $V_L$ to decrease, so $E_o$ cannot increase without limit (*Cuzzi et al.*, 1993) (see also section 3.3.2). Furthermore, in realistic situations, the supply of drifting solids is finite, and this limits the extent to which $E_o$ can grow. More detailed numerical modeling of this process as applied to water (*Ciesla and Cuzzi*, 2005a,b) indicates that enhancements are smaller — typically a factor of 3–30 — for model parameters thus far explored, because of the finite outer nebula source for the enhancement.

There is an initial, transient, regime of interest (regime 1) in which enhanced, evaporated material is found only within a radial band of width determined by the evaporation time of drifting rubble, which is species-dependent. For the peak enhancement to propagate throughout the inner nebula and approach steady state takes a time $t_{ss} \approx R_{ev}/V_n \approx R_{ev}^2/\alpha cH \approx 40/\alpha$ orbit periods. Considering water as the volatile of interest, $R_{ev} \sim 5$ AU and $\alpha \sim 10^{-3}$–$10^{-4}$, $t_{ss} \sim 0.5$–$5$ m.y.; this is long enough to be interesting for chemical variations in the inner nebula due to varying $H_2O$ abundance and associated oxygen fugacity. In steady state, two regimes of interest for C(R) can be distinguished. If $\mathcal{L} \ll 1$ (no sink; regime 2), the entire region inward of $R_{ev}$ is enhanced by $E_o$ over solar. If significant planetesimal growth occurs, leading to a sink and $\mathcal{L} \gg 1$ (regime 3), the inner nebula becomes depleted in the volatile species, with $C/C_o = E_o/(1 + \mathcal{L})$ (the Stevenson and Lunine regime). The regimes are illustrated in Fig. 6. Depending on the rate at which $\mathcal{L}$ grows, the nebula might evolve between these regimes in different ways. Clearly, these are very idealized models, and the process is worthy of future numerical study incorporating accretion. In the next section we highlight other meteoritics applications.

In summary, the essence of this process is that rapid radial drift of meter-sized particles brings mass into the vicinity of an evaporation boundary much faster than it can be removed once it evaporates and becomes coupled to the gas. This is why we refer to it as an *evaporation front*. Its concentration in the gas thus builds significantly. This increased abundance slowly propagates inwards, both by diffusion and by advection with the nebula gas. Formation of a sink at $R_{ev}$ can cause the situation to reverse, with outward diffusion then drying out the inner regions.

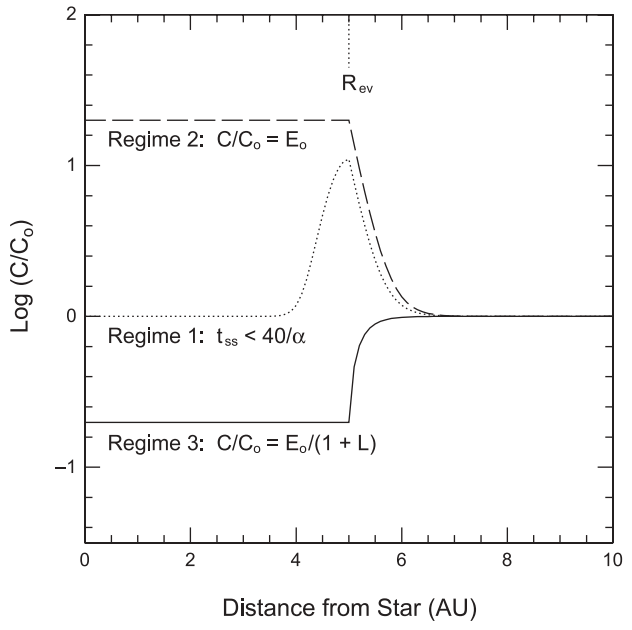


**Fig. 6.** Schematic of the radial (and temporal) variation of enhancement $C/C_o$ for "water" with an evaporation boundary at $R_{ev}$ = 5 AU, taking for illustration a modest $E_o = 20$. In regimes 1 and 2, there is no sink at $R_{ev}$ ($\Lambda = 0$); regime 1 (dotted; schematic only) represents the transient situation, where the inner nebula retains $C/C_o = 1$ for typically $200/\pi\alpha$ orbit periods. Regime 2 (dashed) is the steady-state solution for $\Lambda = 0$. As time proceeds and planetesimals grow in the enhanced solid density outside $R_{ev}$, $\Lambda$ increases; regime 3 (solid) illustrates the steady-state solution for $E_o = 20$ and $\Lambda = 100$.

## 6. SCENARIOS FOR METEORITE PARENT BODIES

Below we present some mental cartoons that illustrate how the physical principles discussed in this chapter might be relevant to parent-body properties. These are intended to be thought-provoking rather than definitive. We expand on these thoughts in *Cuzzi et al.* (2005a).

We start with some of the fundamental challenges of the meteorite data. From studies of thermal histories of ordinary chondrites with different grades of thermal metamorphism, an onion-shell model has arisen (reviewed by *McSween et al.*, 2002; and most recently by *Trieloff et al.*, 2003). Most, if not all, H chondrites of all metamorphic grades are thought to come from a single object that is in the 100-km-radius range, originally composed almost entirely of chondrules of very similar and well-characterized properties; the more deeply buried portions were thermally altered after accretion. While evidence of this sort is somewhat less convincing for other ordinary chondrite types, there is no particular reason to believe their parents, chondrite parents in general, or even the original achondrite parents, should be qualitatively different in this regard. Thus we seek an accretionary process that can construct 100-km bodies out of chondrule-sized particles that are very similar in size and composition within a given parent body, but vary noticeably among parent bodies. The growing evidence for a 1–3-m.y. age gap between CAIs and chondrules [depending on chondrite type; see *Russell et al.* (2006)] is consistent with both the rarity of melted asteroids and the fact that even the oldest achondrites are not measurably older than the oldest chondrules. If chondrules formed with the canonical CAI $^{26}$Al abundance — that is, much earlier than a million years after CAI formation — any object as large as 10 km radius would have melted, at least in its central regions (*Lee et al.*, 1976; *Woolum and Cassen*, 1999). Objects larger than 15 km radius, forming even 0.5 m.y. after CAIs, would have reset the Al-Mg systematics in more than half their volume (*LaTourrette and Wasserburg*, 1998). Larger, observable asteroids in the 100-km-radius range must have waited more than 2 m.y. after CAI formation to avoid large-scale melting (*McSween et al.*, 2002, their Fig. 5; also references therein). All the above constraints neglect the additional heating due to $^{60}$Fe, which now seems more important than previously thought (compare *Bennett and McSween*, 1996, and *Russell et al.*, 2006). Thus, the process by which these parent bodies formed must have waited $10^6$ years or so after CAIs to really get rolling, consistent with observations of the persistence of abundant dust in million-year-old protoplanetary nebulae (*Dullemond and Dominik*, 2005).

If the primary accretion process were too efficient once it started, accretion would complete too quickly for the apparent duration of chondrule and chondrite formation. The diversity of mineralogies seen would rely on spatial, rather than temporal, variations. Because different chondrite types (and apparently different regions of the asteroid belt) have distinct chemical, isotopic, and physical properties, a temporally extended accretionary process must accumulate a given parent body quickly in some sense — that is, before the local gas and solid properties change substantially, and perhaps before chondrules produced in neighboring regions under different conditions can be intermingled (see *Cuzzi et al.*, 2005a, for more discussion).

Chondrites contain mixtures of materials formed in different environments, which argues for significant spatial and/or temporal mixing. Nonequilibrium mineralogies are common in many of these meteorite constituents, and a way must be found to prevent some particles from reaching equilibrium with the gas in which they formed. Fine-grained rims, probably accretionary, envelop pretty much everything in the most primitive, unbrecciated samples. Moreover, 99% of the material in chondrites is isotopically homogeneous in nearly all elements (with the important exception of oxygen). The rare isotopically anomalous grains are ordinarily assumed to be presolar, thus most chondritic silicates seem to have been nebula condensates at some point. These properties are discussed in more detail below.

The first accretion process was incremental accretion from tiny, interstellar grains into a broad, plausibly power-law distribution extending up to a meter or so in size (sec-

tions 3.2 and 3.3.2). The level of turbulence plays a critical role in setting the pace of further particle growth; in even quite low levels of turbulence, growth past the meter-sized range might be greatly slowed, or even precluded (section 3.3.2). Few meter-sized aggregates survive as entities, but probably get collisionally disrupted and reaccreted many times over many years, all the time drifting inward.

### 6.1. Chemical, Mineralogical, and Isotopic Variations Driven by Global Redistribution of Material

If meter-sized particles form quickly, extensive radial redistribution of solid material must have occurred in the early solar system due to their extensive inward radial drift. In combination with this strong mass flow, evaporation fronts, with varying locations, can play a role in enhancing both solid and vapor components of different species relative to each other. More needs to be done to explore the implications of this new complication for meteoritics (sections 5.2–5.4).

The two major volatiles for meteoritics are ferromagnesian silicates ($T_C \approx 1450$ K) and water ($T_C \approx 160$ K). The higher temperature was probably only attained in the innermost solar nebula, early in nebula evolution, when the accretion rate was as high as $10^{-7}$ $M_\odot$/yr or more. *Cuzzi et al.* (2003) have described in some detail a scenario in which primitive, carbon-rich, drifting silicate rubble greatly enhanced the vapor abundance of silicate materials inside $R_{ev}$ (silicates), while the combustion of abundant associated carbon maintained the nebula oxygen fugacity at sufficiently low values to explain the (reduced) mineralogy of CAIs that formed in the region. Estimates of the silicate mass flux that passed through $R_{ev}$ as midplane boulders and evaporated can reach tens of Earth masses over the $10^5$-yr duration of the high-temperature inner nebula phase. The subsequent fate of this very large amount of material has not been modeled. Surely some — perhaps much — was lost into the Sun, but a considerable amount was probably recycled, by outward diffusion or stellar/disk winds, back into cooler regions where it recondensed. Perhaps this abundant reservoir of evaporated and recondensed material can provide the isotopically homogeneous contents of the meteoritic condensates that accreted more than $10^6$ yr later.

The other condensible of interest is water. Solutions presented by *Cuzzi and Zahnle* (2004) (section 5.4) indicate that the warm plume of water vapor created at the water evaporation boundary, or waterline, propagates into the inner solar system on a timescale $\leq 10^6$ yr, bringing with it an enhanced water/hydrogen ratio in the vapor phase. While the analytical solutions of Cuzzi and Zahnle allow enhancements by one or two orders of magnitude, recent numerical modeling by *Ciesla and Cuzzi* (2005a,b) indicates that finite-source and finite-duration factors limit this enhancement to a factor of 3–30 for nebula parameters studied so far. At some point later in time, planetesimal growth just outside the waterline creates a sink that can dry out the inner solar system, leading to water vapor abundances far lower than nominal cosmic. Strongly time- or location-dependent water vapor abundance might help account for the varying FeO abundances in different chondrite components (*Palme and Fegley,* 1990; *Fedkin and Grossman,* 2004). Forming FeO-rich silicates requires nebula oxygen fugacity higher than nominal; on the other hand, forming enstatite chondrites requires oxygen fugacity lower than nominal. Another possible application is the aqueously altered fine-grained material that rims chondrules and other objects in CM chondrites (*Metzler et al.,* 1992). Many believe that these grains can only have been altered on the parent body by liquid water; however, *Ciesla et al.* (2003) argue that nebula shocks can aqueously alter isolated fine-grained silicate particles in the nebula, if the water abundance is enhanced over solar in the nebula gas by a factor of about 100.

This effect might also help us understand mass-independent oxygen-isotopic fractionations. If the $^{17}O$ and $^{18}O$ isotopes are preferentially exchanged from CO to water molecules by photodissociation in the parent molecular cloud, or in the rarified upper reaches of the nebula, the early inner nebula where CAIs formed would have been elevated in $^{16}O$ until sufficient $^{17}O$ and $^{18}O$-rich icy material drifted inward to change the relative abundance (*Yurimoto and Kuramoto,* 2004; *Krot et al.,* 2005b) (cf. sections 5.2–5.4). In this case, correlations between oxygen fugacity and oxygen-isotopic content would be expected. *Yurimoto and Kuramoto* (2004) argue that only a factor of several enhancement in water is needed.

Future work might profitably address how other interesting volatiles such as FeS, or metallic Fe, might behave. Another interesting angle to pursue in this regard might be the volatility-dependent abundance variations seen in moderately volatile elements in all chondrites (*Cassen,* 2001; *Alexander et al.,* 2001).

The strong redistribution of volatiles resulting from radial drift of solids past evaporation boundaries might be observable by remote astronomical observations; enhancements of CO have been found in actively accreting disks out to several AU from the star (*Najita et al.,* 2003) — perhaps without the expected amount of water (*Carr et al.,* 2004).

### 6.2. Radial Mixing of Small Particles After Formation

Inward drift of large particles is not the only way solids can be redistributed globally. The mixture in primitive meteorites of high-temperature condensates manifesting solar (or lower) oxygen fugacity (CAIs), and lower-temperature condensates manifesting much higher oxygen fugacity (some chondrules, most matrix) — not to mention their age and isotopic differences — has always been a puzzle. Some of the appeal of the stellar wind models for CAI and chondrule formation comes from their potential ability to transport particles directly from regions where the temperature

is known to be high enough to melt rocks, to regions where they may accrete. Temporal mixing is another possibility, in principle; CAIs might form at an earlier, higher-temperature epoch, but in the same radial region as chondrules later form and accrete.

It has been a widespread and persistent concern that CAI-sized particles cannot survive in the nebula for the apparent time difference between them and most chondrules, because of their radial drift due to gas drag (section 2.4, Fig. 1). This has even led some to question the reality of the age difference. This concern is traceable to early work by *Weidenschilling* (1977), who quoted drift rates for small particles in a nonturbulent nebula (see section 2.4.1); however, Weidenschilling had included caveats about turbulence, and *Morfill* (1983) argued qualitatively for the vigor of turbulent diffusion of particles.

Recently, *Cuzzi et al.* (2003) showed quantitatively how turbulent diffusion can transport CAIs outward from an inner solar system source to asteroidal distances, and allow them to survive in appropriate abundances for 1–3 m.y. This happens because outwardly radial diffusive mass flux can be as large as inwardly radial gas drag drift flux, in the presence of an outward concentration gradient such as would exist if CAIs were only created in the inner solar system. Tiny grains have the slowest inward drift and are the most easily transported outward by turbulent diffusion. Simple diffusion is capable of explaining outward radial mixing of 1–10-μm-sized crystalline silicate grains in cometary IDPs (*Bockelée-Morvan et al.*, 2002); tiny refractory grains might be mixed outward from the innermost nebula diffusively into comet formation regions, as well as by stellar wind ejection. *Harker and Desch* (2002) suggest that crystalline silicates are formed in the outer nebula by annealing in spiral density waves, and *Boss* (2004) has shown that such waves can themselves produce significant radial mixing even in the absense of diffusive turbulence.

Because larger particles in this size range have faster inward radial drift rates than smaller ones (section 2.4.1), it is somewhat more difficult for diffusion to retain the larger particles; *Cuzzi et al.* (2003) showed that centimeter-sized CAIs could be diffused to the asteroid belt region, but that they disappeared more quickly than the smaller, more ubiquitous millimeter-sized CAIs (which also have different mineralogical and chemical properties). They therefore predicted that the meteorites containing the largest CAIs (CV chondrites) would thus need to have accreted earlier than other meteorite types. It is consistent with this argument that CVs contain not only the largest CAIs, but also the largest AOAs, which are nearly as old but clearly formed in somewhat cooler regions. Some preliminary data is consistent with this prediction (*Amelin et al.*, 2004; *Bizzarro et al.*, 2004; see *Russell et al.*, 2006). Age-dating techniques should be able to test this prediction in the near future.

Some minerals in chondritic particles (all CAIs and AOAs, for instance) are not in their equilibrium state — as if they had not had time to equilibrate with their cooling parent gas before being transported into cooler regions (e.g., *Wood*, 2004). Future studies of minerals found in non-equilibrium states might be able to distinguish between different hypotheses for outward transport of CAIs from hot, inner creation regions to the asteroid belt. Minerals undergo a condensation-reaction sequence as they traverse a cooling gas. If transport is by stellar wind ejection, it occurs almost instantaneously (on an orbital timescale) and at very low density. If outward radial transport is by diffusion, it occurs on a considerably longer timescale. Minerals react slowly with the gas phase, and the kinetics of these reactions are not well understood. Solid-state diffusion coefficients are only known for a limited range of cases and are strongly temperature dependent (e.g., *LaTourrette and Wasserburg*, 1998); however, reaction times could well be in the $10^3$–$10^4$-yr range, depending on the thermal profile experienced by the evolving particle. This subject is covered in more detail by *Cuzzi et al.* (2005a,b).

### 6.3. Fine-grained Rims: Accretion and/or Erosion

As small, solid particles such as chondrules and CAIs move through the nebula gas, they constantly encounter finer-grained material, both as monomers and as fractal aggregates of monomers, which are more firmly coupled to the gas. Depending on the relative velocity of encounter, these grains might stick to, compress, or erode the granular surfaces of the chondrules and CAIs. *Cuzzi* (2004) has modeled accretion rims on chondrules and CAIs. Using quantitative modeling of relative velocities of particles in gas turbulence, and using sticking outcomes based on the theory of *Dominik and Tielens* (1997), chondrule-sized particles are found to accrete fairly compact rims of fine-grained material in times of $10^3$–$10^4$ yr depending on the relative abundances of chondrules and dust. This model explains how chondrule rims can be fairly compact, with thicknesses nearly proportional to the size of the underlying chondrule (as found by *Metzler et al.*, 1992; *Paque and Cuzzi*, 1997) under plausible conditions of weak nebula turbulence, as long as all chondrules in the same parent body share approximately the same rim accretion time. Some cautionary comments are presented by *Wasson et al.* (2005). One easy way to understand how this can happen is if the chondrules in a region sweep up all the dust in the region, as suggested by *Morfill et al.* (1998). *Cuzzi* (2004) shows that the detailed form of the dependence of rim thickness on core particle size (nearly linear) might be a third indicator that chondrule-sized particles are of the right size for turbulent concentration to act on them (cf. section 4). More measurements of rim thicknesses in different chondrite types would be useful.

Fine-grained accretionary rims on CAIs are prevalent, and many CAI accretion rims show clear affiliations with the nebula regime in which the CAIs themselves formed (*Krot et al.*, 2002) lying beneath rims from the environment in which chondrules formed (*MacPherson et al.*, 1985).

Calcium-aluminum-rich inclusion accretion rims studied to date are much thinner, relative to their core particle size, than fine-grained rims on chondrules in the same chondrites. *Cuzzi* (2004) suggests that this is because the CAIs with the most obvious fine-grained rims are larger than chondrules, and would be expected to have correspondingly larger velocities relative to the gas and coupled fine grains, which may erode, rather than accrete onto, their surfaces. Especially in an erosive regime, protected hollows in complex surfaces will preferentially accumulate material, such as is often seen in CAIs (*MacPherson et al.*, 1985; *Krot et al.*, 2002). This could be studied more using CAIs with sizes closer to those of chondrules. These differences would have to be reconciled with sorting together in the same meteorite of these CAIs and chondrules, which also depends on their stopping time $t_s$.

This scenario would seem to be consistent with the general observation that chondrule fine-grained rim material is similar in composition to (if somewhat smaller in size than) matrix grains in the same chondrites (*Scott et al.*, 1989; *Ashworth*, 1977) and complementary to the chemistry of the chondrule cores themselves in the sense that iron and other volatiles lost from chondrules are complemented in their rims and matrix (*Wood*, 1985). More studies of rim-matrix relationships would be valuable.

By contrast, the concept that chondrules and CAIs acquire their rims in high-speed stellar winds (*Liffman and Toscano*, 2000) seems rather unlikely. The relative velocities involved are estimated as the terminal velocity of the grain, under solar gravity, in the very low density wind: $V_T \sim g t_s$. Recall from section 5.1 that $t_s \sim \Omega_x^{-1} \sim 10^5$ s; thus anywhere inside 2 AU, $V_T \sim 1$ km/s. This velocity is hard to reconcile with sticking of grains and much more likely to result in net erosion of rims, if not pitting and erosion of the igneous object itself.

### 6.4. Primary Accretion

By primary accretion, we refer to the process by which primitive planetesimals having the size and content of meteorite parent bodies were put together from the individual components discused above. These are objects large enough to escape gas-drag-driven drift loss "into the Sun," and to have identifiable macroscopic-to-megalithic properties that are connected to their nebula precursors, but small enough that they have escaped melting, preserving the primary characteristics of their nebular constituents. Inferring the true "primary" characteristics from the current crop of meteorites requires us to look backward through a number of planetary processes — collisions, grinding, abrasion, thermal and aqueous alteration, etc. (cf. *Weidenschilling*, 2006). Here we speculate on only the very earliest stages of primary accretion. Some of these speculations are pursued further in *Cuzzi et al.* (2005a).

As mentioned above, several arguments support a 1–3-m.y. hiatus between the earliest days of the solar system (the formation of CAIs) and the primary accretion of the parent bodies of most of our meteorites (*Russell et al.*, 2006). It seems to us that maintaining a small amount of turbulence ($10^{-5} < \alpha < 10^{-2}$) in the inner solar system throughout most of this time is the most obvious way to account for this (section 3.3.2). The situation in the outer nebula might have been different; the need to preserve the limited amount of solid material there by making accretion easier easier and faster might lead one to believe that turbulence there was much weaker (*Weidenschilling*, 1997). However, current estimates suggest that the magnetorotational instability is easily capable of making the entire outer nebula turbulent (*Sano et al.*, 2000). If the outer nebula were turbulent, turbulent concentration might have played a role in fostering planetesimal growth (cf. section 4, Fig. 3). Evidence for this might be hard to find.

In 1–3 m.y., the nebula evolves dramatically, losing most of its initial mass, dropping to a much lower accretion rate and a much lower photospheric and magnetospheric activity level overall, and cooling at all radial locations. Evaporation fronts move, possibly by several AU, as a result of this evolution. The minimum mass nebula with which most planetary accumulation models start, often identified with the revealed stage of T Tauri star evolution, is only a mere shadow of its former self. Once primary accretion starts, one has the (poorly quantified) impression that it happens quickly. Why was primary accretion delayed for over a million years, until after chondrules formed, and yet proceeded with alacrity thereafter?

Given the prevailing expectation that Jupiter itself formed on the 1–3-m.y. timescale, one must at least consider what influence the formation of Jupiter (by this we mean the rapid accretion of its massive gaseous envelope) might have had on the asteroid-formation region. For example, nebula shock waves driven into the inner solar system by the fully formed Jupiter might both have melted the chondrules and influenced the local level of turbulence (more likely to have increased it, than to have decreased it).

A possibility favored by S.J.W. is that decreasing gas density (due to nebula evolution into the Sun) and decreasing opacity (due to accretion) might have led to a substantial cutoff in turbulence at some stage. In section 3.3.1 we showed how sensitive the accretion rate is to $\alpha$ decreasing below a certain (very low) threshold value ($<10^{-6}$–$10^{7}$) at which point the particle layer becomes self-shielded from the nebula headwind. In this scenario, formation of Jupiter perturbs some planetesimals into eccentric orbits crossing large radial regions, causing bow shocks that generate the chondrules we now see, which, because turbulence is low, accrete quickly. Under this scenario one would need to understand how the distinct parent bodies of the different chondrite classes could be formed, with such well-determined chemical properties and size-density sorting characteristics. Furthermore, the turbulence threshold required for this to occur is extremely low. While it is widely believed that differential rotation alone cannot maintain continuous

turbulence, this question is far from settled at the extremely low levels of $\alpha$ that permit rapid midplane accretion (section 2.1).

A different possibility, favored by J.N.C., is that weak turbulence was ongoing and ubiquitous, allowing growth only to meter size, until some confluence of events (perhaps also involving Jupiter's formation) led to chondrule formation and turbulent concentration. The decreasing gas density and varying turbulent intensity might have only then reached combinations (Fig. 3) at which chondrules and their like could incur significant concentration to leapfrog the meter-sized particle barrier that frustrates incremental accretion in turbulence. For an extended time, these processes sporadically produced dense, if not fully packed, protoplanetesimals that continued to compact under collisional and gravitational processes (section 4). Turbulent concentration does present the advantage of allowing small variations in local gas density, or $\alpha$, or both to determine the properties of the mineral objects that are subjected to strong concentration (sections 4 and 6.3). This scenario predicts widespread radial mixing of chondrite constituents prior to their accretion, which must be reconciled with the distinct properties of the meteorite classes (see *Cuzzi et al.*, 2005a).

The challenge remains to end up with planetesimals made out of the rocks we have in our collections — plausibly, 100-km-radius objects, each composed almost entirely of millimeter-sized components with well-defined properties, but varying noticeably from one to another. It has been a widespread assumption that the chondrite and asteroid groups represent spatial variation at some nominal point in time; however, the alternate must be considered that chondrite groups represent temporal (but still local) grab samples of an evolving nebula mix, or perhaps at least a combination of both spatial and temporal variations. One must also keep in mind that the current crop of meteorite types remains a biased and incomplete sample of what exists out in the asteroid belt. As only one example, a set of Antarctic meteorites has recently been identified as H chondrites, but they incorporate abundant CAIs (rare in normal H chondrites) and possess a matrix like that seen in CO chondrites (*Kimura et al.*, 2002)! Clearly there is a lot to learn, and, while progress is being made in understanding different components of the process, we remain a long way from any coherent scenario of meteorite parent-body formation.

***Acknowledgments.*** We are grateful to many colleagues for helping educate us over the years to the nuances of the meteorite record, against which any theory must be judged. In the context of this specific chapter, we have benefitted from conversations with J. Beckett, L. Grossman, J. Paque Heather, M. Humayan, A. Krot, A. Meibom, S. Russell, and E. Scott. In the theoretical areas we have benefitted from useful conversations with P. Cassen, L. Hartmann, and K. Zahnle, and helpful internal reviews by K. Zahnle, I. Mosqueira, and P. Estrada. We thank our three reviewers for their careful reading of the chapter, and the editors for their flexibility regarding length. Contributions of J.N.C. were supported by grants from NASA's Planetary Geology and Geophysics and Origins of Solar Systems programs. Research of S.J.W. was supported by NASA grant NAG5-13156. This chapter has made ample use of the invaluable ADS Astronomy/Planetary Abstract Service.

## REFERENCES

Ackridge G. and Sears D. W. G. (1998) Chondrule and metal size-sorting in asteroidal regoliths: Experimental results with implications for chondrites (abstract). In *Lunar and Planetary Science XXIX*, pp. 1198–1199. Lunar and Planetary Institute, Houston.

Adachi I., Hayashi C., and Nakazawa K. (1976) The gas drag effect on the elliptical motion of a solid body in the primordial solar nebula. *Prog. Theor. Phys., 56*, 1756–1771.

Afshordi N., Mukhopadhyay B., and Narayan R. (2005) Bypass to turbulence in hydrodynamic accretion: Lagrangian analysis of energy growth. *Astrophys. J., 629*, 373–382.

Alexander C. M. O'D., Boss A. P., and Carlson R. W. (2001) Early evolution of the inner solar system: A meteoriticist's perspective. *Science, 293*, 64–68.

Amelin Y., Krot A. N., Hutcheon I. D., and Ulyanov A. A. (2002) Lead isotopic ages of chondrules and calcium-aluminum-rich inclusions. *Science, 297*, 1678–1683.

Amelin Y., Krot A. N., Hutcheon I. D., and Ulyanov A. A. (2004) Duration of the chondrule formation interval; a Pb isotope study (abstract). In *Planetary Timescales: From Stardust to Continents*, February 2004, Canberra, Australia.

Anderson J. M., Li Z.-Y., Krasnopolsky R., and Blandford R. D. (2003) Locating the launching region of T Tauri winds: The case of DG Tauri. *Astrophys. J. Lett., 590*, L107–L110.

André P., Ward-Thompson D., and Barsony M. (2000) From prestellar cores to protostars: The initial conditions of star formation. In *Protostars and Planets* (V. Mannings et al., eds.), pp. 589–612. Univ. of Arizona, Tucson.

Arldt R. and Urpin V. (2004) Simulations of vertical shear instability in accretion disks. *Astron. Astrophys., 426*, 755–765.

Ashworth J. R. (1977) Matrix textures in unequilibrated ordinary chondrites. *Earth Planet. Sci. Lett., 35*, 25–34.

Barranco J. and Marcus P. (2004) Three-dimensional vortices in protoplanetary disks. *Astrophys. J., 623*, 1157–1170.

Barge P. and Sommeria J. (1995) Did planet formation begin inside persistent gaseous vortices? *Astron. Astrophys., 1*, L1–L4.

Bell K. R., Cassen P. M., Klahr H. H., and Henning Th. (1997) The structure and apeparance of protostellar accretion disks: Limits on disk flaring. *Astrophys. J., 486*, 372–387.

Bennett M. E. and McSween H. Y. Jr. (1996) Revised model calculations for the thermal histories of ordinary chondrite parent bodies. *Meteoritics & Planet. Sci., 31*, 783–792.

Bizzarro M., Baker J. A., and Haack H. (2004) Mg isotopic evidence for contemporaneous formation of chondrules and refractory inclusions. *Nature, 431*, 275–278.

Blum J. (2000) Laboratory experiments on preplanetary dust aggregation. *Space Sci. Rev., 192*, 265–278.

Blum J. (2004) Grain growth and coagulation. In *Astrophysics of Dust* (A. N. Witt et al., eds.), pp. 369–391. ASP Conference Series 309, Astronomical Society of the Pacific, San Francisco.

Blum J. and Schräpler R. (2004) Structure and mechanical properties of high-porosity macroscopic aggregates formed by random ballistic deposition. *Phys. Rev. Lett., 93*, 115503–1 to 115503–4.

Blum J. and Wurm G. (2000) Experiments on sticking, restructuring, and fragmentation of preplanetary dust aggregates. *Icarus, 143,* 138–146.

Bockelée-Morvan D., Gautier D., Hersant F., Huré J.-M., and Robert F. (2002) Turbulent radial mixing in the solar nebula as the source of crystalline silicates in comets. *Astron. Astrophys., 384,* 1107–1118.

Boley A. C., Durisen R. H., and Pickett M. K. (2005) The three-dimensionality of spiral shocks: Did chondrules catch a breaking wave? In *Chondrites and the Protoplanetary Disk* (A. N. Krot et al., eds.), pp. 839–848. ASP Conference Series 341, Astronomical Society of the Pacific, San Francisco.

Boss A. P. (2004) Evolution of the solar nebula. VI. Mixing and transport of isotopic heterogeneity. *Astrophys. J., 616,* 1265–1277.

Boss A. P. and Goswami J. N. (2006) Presolar cloud collapse and the formation and early evolution of the solar nebula. In *Meteorites and the Early Solar System II* (D. S. Lauretta and H. Y. McSween Jr., eds.), this volume. Univ. of Arizona, Tucson.

Bracco A., Provenzale A., Spiegel E. A., and Yecko P. (1998) Spotted disks. In *Theory of Black Hole Accretion Disks* (A. Marek et al., eds.), p. 254. Cambridge Univ., Cambridge.

Busse F. (2004) Visualizing the dynamics of the onset of turbulence. *Science, 305,* 1574–1575.

Calvet N., Hartman L., and Strom S. E. (2000) Evolution of disk accretion. In *Protostars and Planets* (V. Mannings et al., eds.), pp. 377–400. Univ. of Arizona, Tucson.

Carballido A., Stone J. M., and Pringle J. E. (2005) Diffusion coefficient of a passive contaminant in a local MHD model of a turbulent accretion disk. *Mon. Not. R. Astron. Soc., 358,* 1055–1060.

Carr J. S., Tokunaga A. T., and Najita J. (2004) Hot $H_2O$ emission and evidence for turbulence in the disk of a young star. *Astrophys. J., 603,* 213–220.

Cassen P. M. (2001) Nebular thermal evolution and the properties of primitive planetary materials. *Meteoritics & Planet. Sci., 36,* 671–700.

Champney J. M., Dobrovolskis A. R., and Cuzzi J. N. (1995) A numerical turbulence model for multiphase flow in a non-equilibrium protoplanetary nebula. *Phys. Fluids, 7,* 1703–1711.

Chaussidon M. and Gounelle M. (2006) Irradiation processes in the early solar system. In *Meteorites and the Early Solar System II* (D. S. Lauretta and H. Y. McSween Jr., eds.), this volume. Univ. of Arizona, Tucson.

Chokshi A., Tielens A. G. G. M., and Hollenbach D. (1993) Dust coagulation. *Astrophys. J., 407,* 806–819.

Ciesla F. J. and Cuzzi J. N (2005a) The distribution of water in a viscous protoplanetary disk (abstract). In *Lunar and Planetary Science XXXVI,* Abstract #1479. Lunar and Planetary Institute, Houston (CD-ROM).

Ciesla F. J. and Cuzzi J. N. (2005b) The evolution of the water distribution in a viscous protoplanetary disk. *Icarus,* in press.

Ciesla F., Lauretta D. S., Cohen B. A., and Hood L. L. (2003) A nebular origin for chondritic fine-grained phyllosilicates. *Science, 299,* 549–552.

Clarke C. J. and Pringle J. E. (1988) The diffusion of contaminant through an accretion disk. *Mon. Not. R. Astron. Soc., 235,* 365–373.

Clift R., Grace J. R., and Weber M. E. (1978) *Bubbles, Drops, and Particles.* Academic, New York. 380 pp.

Connolly H. C. Jr., Desch S. J., Chiang E., Ash R. D., and Jones R. H. (2006) Transient heating events in the protoplanetary nebula. In *Meteorites and the Early Solar System II* (D. S. Lauretta and H. Y. McSween Jr., eds.), this volume. Univ. of Arizona, Tucson.

Cuzzi J. N. (2004) Blowing in the wind: III. Accretion of dust rims by chondrule-sized particles in a turbulent protoplanetary nebula. *Icarus, 168,* 484–497.

Cuzzi J. N., Petaev M., Ciesla F. J., Krot A. N., Scott E. R. D., and Weidenschilling S. J. (2005a) History of thermally processed solids: Reconciling models and meteoritics. In *Chondrites and the Protoplanetary Disk* (A. N. Krot et al., eds.). ASP Conference Series, in press.

Cuzzi J. N., Petaev M., Ciesla F. J., Krot A. N., and Scott E. R. D. (2005b) Nebula models of non-equilibrium mineralogy: Wark-Lovering rims (abstract). In *Lunar and Planetary Science XXXVI,* Abstract #2095. Lunar and Planetary Institute, Houston (CD-ROM).

Cuzzi J. N., Davis S. S., and Dobrovolskis A. R. (2003) Blowing in the wind: II. Creation and redistribution of refractory inclusions in a turbulent protoplanetary nebula. *Icarus, 166,* 385–402.

Cuzzi J. N., Dobrovolskis A. R., and Champney J. M. (1993) Particle-gas dynamics near the midplane of a protoplanetary nebula. *Icarus, 106,* 102–134.

Cuzzi J. N., Dobrovolskis A. R., and Hogan R. C. (1994) What initiated planetesimal formation? (abstract). In *Lunar and Planetary Science XXV,* pp. 307–308. Lunar and Planetary Institute, Houston.

Cuzzi J. N., Dobrovolskis A. R., and Hogan R. C. (1996) Turbulence, chondrules, and planetesimals. In *Chondrules and the Protoplanetary Disk* (R. Hewins et al., eds.), pp. 35–44. Cambridge Univ., Cambridge.

Cuzzi J. N. and Hogan R. C. (2003) Blowing in the wind: I. Velocities of chondrule-sized particles in a turbulent protoplanetary nebula. *Icarus, 164,* 127–138.

Cuzzi J. N., Hogan R. C., and Paque J. M. (1999) Chondrule size density distributions: Predictions of turbulent concentration and comparison with chondrules disaggregated from L4 ALH85033 (abstract). In *Lunar and Planetary Science XXX,* Abstract #1274. Lunar and Planetary Institute, Houston (CD-ROM).

Cuzzi J. N., Hogan R. C., Paque J. M., and Dobrovolskis A. R. (2001) Size-selective concentration of chondrules and other small particles in protoplanetary nebula turbulence. *Astrophys. J., 546,* 496–508.

Cuzzi J. N. and Zahnle K. R. (2004) Material enhancement in protoplanetary nebulae by particle drift through evaporation fronts. *Astrophys. J., 614,* 490–496.

Cyr K., Sears W. D., and Lunine J. I. (1998) Distribution and evolution of water ice in the solar nebula: Implications for solar system body formation. *Icarus, 135,* 537–548.

Cyr K., Sharp C. M., and Lunine J. I. (1999) Effects of the redistribution of water in the solar nebula on nebular chemistry. *J. Geophys. Res., 104,* 19003–19014.

Davis S. S., Sheehan D. P., and Cuzzi J. N. (2000) On the persistence of small regions of vorticity in the protoplanetary nebula. *Astrophys. J., 545,* 494–503.

Desch S. and Cuzzi J. N. (2000) Formation of chondrules by lightning in the protoplanetary nebula. *Icarus, 143,* 87–105.

Dobrovolskis A. R., Dacles-Mariani J. M., and Cuzzi J. N. (1999) Production and damping of turbulence in the solar nebula. *J. Geophys. Res.–Planets, 104,* 30805–30815

Dodd R. T. (1976) Accretion of the ordinary chondrites. *Earth Planet. Sci. Lett., 30,* 281–291.

Dominik C. and Tielens A. G. G. M. (1997) The physics of dust coagulation and the structure of dust aggregates in space. *Astrophys. J., 480,* 647–673a.

Dominik C. P., Blum J., Cuzzi J. N., and Wurm G. (2006) Growth of dust as initial step towards planet formation. In *Protostars and Planets V* (B. Reipurth et al., eds.). Univ. of Arizona, Tucson, in press.

Dubrulle B., Morfill G. E., and Sterzik M. (1995) The dust subdisk in the protoplanetary nebula. *Icarus, 114,* 237–246.

Dullemond C. P. and Dominik C. (2005) Dust coagulation in protoplanetary disks: A rapid depletion of small grains. *Astron. Astrophys., 434,* 971–986.

Eaton J. K. and Fessler J. R. (1994) Preferential concentration of particles by turbulence. *Intl. J. Multiphase Flow, Suppl., 20,* 169–209.

Fedkin A. V. and Grossman L. (2004) Nebular formation of fayalitic olivine: Ineffectiveness of dust enrichment (abstract). In *Lunar and Planetary Science XXXV,* Abstract #1823. Lunar and Planetary Institute, Houston (CD-ROM).

Fleming T. and Stone J. M. (2003) Local magnetohydrodynamic models of layered accretion disks. *Astrophys. J., 585,* 908–920.

Frohn A. and Roth N. (2000) *Dynamics of Droplets.* Springer, Berlin. 292 pp.

Fromang S. and Nelson R. P. (2005) On the accumulation of solid bodies in global turbulent protoplanetary disk models. *Mon. Not. R. Astron. Soc.,* in press.

Garaud P. and Lin D. N. C. (2004) On the evolution and stability of a protoplanetary disk dust layer. *Astrophys. J., 608,* 1050–1075.

Garaud P. and Ogilvie G. I. (2005) A model for the nonlinear dynamics of turbulent shear flows. *J. Fluid Mech., 530,* 145–176.

Godon P. and Livio M. (2000) The formation and role of vortices in protoplanetary disks. *Astrophys. J., 537,* 396–404.

Goldreich P. and Ward W. R. (1973) The formation of planetesimals. *Astrophys. J., 183,* 1051–1061.

Gomez G. C. and Ostriker E. C. (2005) The effect of the Coriolis force on Kelvin-Helmholz-driven mixing in protoplanetary disks. *Astrophys. J.,* in press.

Goodman J and Pindor B. (2000) Secular instability and planetesimal formation in the dust layer. *Icarus, 148,* 537–549.

Greshake A., Krot A. N., Meibom A., Weisberg M. K., Zolensky M. E., and Keil K. (2002) Heavily-hydrated lithic clasts in CH chondrites and the related, metal-rich chondrites QUE94411 and Hammadah al Hamra 237. *Meteoritics & Planet. Sci., 37,* 281–293.

Haack H. and Scott E. R. D. (1993) Nebula formation of the H, L, and LL parent bodies from a single batch of chondritic materials. *Meteoritics, 28,* 358.

Haghighipour N. and Boss A. P. (2003a) On pressure gradients and rapid migration of solids in a non-uniform solar nebula. *Astrophys. J.., 583,* 996–1003.

Haghighipour N. and Boss A. P. (2003b) On gas drag-induced rapid migration of solids in a nonuniform solar nebula. *Astrophys. J., 598,* 1301–1311.

Harker D. E. and Desch S. J. (2002) Annealing of silicate dust by nebular shocks at 10 AU. *Astrophys. J. Lett., 565,* L109–L112.

Hartmann L. and Calvet N. (1995) Observational constraints on FU Ori winds. *Astrophys. J., 109,* 1846–1855.

Hartmann W. K. (1985) Impact experiments 1. Ejecta velocity distributions and related results from regolith targets. *Icarus, 63,* 69–98.

Hayashi C. (1981) Structure of the solar nebula, growth and decay of magnetic fields and effects of magnetic and turbulent viscosities on the nebula. *Prog. Theor. Phys. Suppl., 70,* 35–53.

Hayashi C., Nakazawa K., and Nakagawa Y. (1985) Formation of the solar system. In *Protostars and Planets II* (D. C. Black and M. S. Matthews, eds.), pp. 1100–1153. Univ. of Arizona, Tucson.

Hogan R. C. and Cuzzi J. N. (2001) Stokes and Reynolds number dependence of preferential particle concentration in simulated 3D turbulence. *Phys. Fluids, 13,* 2938–2945.

Hogan R. C. and Cuzzi J. N. (2005) A cascade model for particle concentration and enstrophy in fully developed turbulence with mass loading feedback. *Phys. Rev. E.,* in press.

Hogan R. C., Cuzzi J. N., and Dobrovolskis A. R. (1999) Scaling properties of particle density fields formed in turbulent flows. *Phys. Rev. E, 60,* 1674–1680.

Huang S., Akridge G., and Sears D. W. G. (1996) Metal-silicate fractionation in the surface layers of accreting planetesimals: Implications for the formation of ordinary chondrites and the nature of asteroid surfaces. *J. Geophys. Res., 101,* 29373–29385.

Hughes D. W. (1978) A disaggregation and thin section analysis of the size and mass distribution of the chondrules in the Bjurbole and Chainpur meteorites. *Earth Planet. Sci. Lett., 38,* 391–400.

Hughes D. W. (1980) The dependence of chondrule density on chondrule size. *Earth Planet. Sci. Lett., 51,* 26–28.

Ishitsu N. and Sekiya M. (2002) Shear instabilities in the dust layer of the solar nebula III. Effects of the Coriolis force. *Earth Planets Space, 54,* 917–926.

Ishitsu N. and Sekiya M. (2003) The effects of the tidal force on shear instabilities in the dust layer of the solar nebula. *Icarus, 165,* 181–194.

Johansen A., Klahr H., and Henning Th. (2005) Gravoturbulent formation of planetesimals. *Astrophys. J.,* in press.

Kempf S., Pfalzner S., and Henning T. (1999) N-particle simulations of dust growth 1. Growth driven by brownian motion. *Icarus, 141,* 388–398.

Kerridge J. F. and Matthews M. S., eds. (1988) *Meteorites and the Early Solar System.* Univ. of Arizona, Tucson. 1269 pp.

Kimura M., Hiyagon H., Palme H., Spettel B., Wolf D., Clayton R. N., Mayeda T. K., Sato T., Suzuki A., and Kojima H. (2002) Yamato 792947, 793408, and 82038: The most primitive H chondrites, with abundant refractory inclusions. *Meteoritics & Planet. Sci., 37,* 1417–1434.

Klahr H. H. and Bodenheimer P. (2003a) Turbulence in accretion disks: Vorticity generation and angular momentum transport via the global baroclinic instability. *Astrophys. J., 582,* 869–892.

Klahr H. H. and Bodenheimer P. (2003b) The formation of a planet in the eye of a hurricane — A three phase model for planet formation (abstract). In *Abstracts for the 35th AAS/DPS Meeting,* Abstract #25.01.

Königl A. and Pudritz R. (2000) Disk winds and the accretion-outflow connection. In *Protostars and Planets IV* (V. Mannings et al., eds.), pp. 759–788. Univ. of Arizona, Tucson.

Kornet K., Stepinski T. F., and Rozyczka M. (2001) Diversity of planetary systems from evolution of solids in protoplanetary disks. *Astron. Astrophys., 378,* 180–191.

Krot A. N., Rubin A. E., Keil K., and Wasson J. (1997) Microchondrules in ordinary chondrites: Implications for chondrule formation. *Geochim. Cosmochim. Acta, 61,* 463–473.

Krot A. N., McKeegan K. D., Leshin L. A., MacPherson G. J., and Scott E. R. D. (2002) Existence of an $^{16}$O-rich gaseous

reservoir in the solar nebula. *Science, 295,* 1051–105.

Krot A. N., Amelin Y., Cassen P., and Meibom A. (2005a) Young chondrules in CB chondrites from a giant impact in the early solar system. *Nature, 436,* 989–992.

Krot A. N., Hutcheon I. D., Yurimoto H., Cuzzi J. N., McKeegan K. D., Scott E. R. D., Libourel G., Chaussidon M., Aleon J., and Petaev M. I. (2005b) Evolution of oxygen isotopic composition in the inner solar nebula. *Astrophys. J., 622,* 1333–1342.

Kuebler K. E., McSween H. Y. Jr., Carlson W. D., and Hirsch D. (1999) Sizes and masses of chondrules and metal-troilite grains in ordinary chondrites: Possible implications for nebular sorting. *Icarus, 141,* 96–106.

LaTourrette T. and Wasserburg G. J. (1998) Mg diffusion in anorthite: Implications for the formation of early solar system planetesimals. *Earth Planet. Sci. Lett., 158,* 91–108.

Lee T., Papanastassiou D. A., and Wasserburg G. J. (1976) Demonstration of $^{26}$Mg excess in Allende and evidence for $^{26}$Al. *Geophys. Res. Lett., 3,* 109–112.

Leenhouts J. M. and Skinner W. R. (1991) Shape-differentiated size distributions of chondrules in type 3 ordinary chondrites. *Meteoritics, 26,* 363.

Liffman K. and Brown M. (1995) The motion and size sorting of particles ejected from a protostellar accretion disk. *Icarus, 116,* 275–290.

Liffman K. and Toscano M. (2000) Chondrule fine-grained mantle formation by hypervelocity impact of chondrules with a dusty gas. *Icarus, 143,* 106–125.

Love S. G. and Ahrens T. (1996) Catastrophic impacts on gravity dominated asteroids. *Icarus, 124,* 141–155.

MacPherson G. J., Hashimoto A., and Grossman L. (1985) Accretionary rims on Allende inclusions: Clues to the accretion of the Allende parent body. *Geochim. Cosmochim. Acta, 49,* 2267–2279.

Markiewicz W. J., Mizuno H., and Völk H. J. (1991) Turbulence-induced relative velocity between two grains. *Astron. Astrophys., 242,* 286–289.

Marshall J. and Cuzzi J. N. (2001) Electrostatic enhancement of coagulation in protoplanetary nebulae (abstract). In *Lunar and Planetary Science XXXII,* Abstract #1262. Lunar and Planetary Institute, Houston (CD-ROM).

Marshall J., Sauke T. B., and Cuzzi J. N. (2005) Microgravity studies of aggregation in particulate clouds. *Geophys. Res. Lett., 32,* L11202.

May C., Russell S. S., and Grady M. M. (1999) Analysis of chondrule and CAI size and abundance in CO3 and CV3 chondrites: A preliminary study (abstract). In *Lunar and Planetary Science XXX,* Abstract #1688. Lunar and Planetary Institute, Houston (CD-ROM).

McSween H. Y., Ghosh A., Grimm R. E., Wilson L., and Young E. D. (2002) Thermal evolution models of asteroids. In *Asteroids III* (W. F. Bottke Jr. et al., eds.), pp. 559–571. Univ. of Arizona, Tucson.

Meneveaux C. and Sreenivasan K. R. (1987) Simple multifractal cascade model for fully developed turbulence. *Phys. Rev. Lett., 59,* 1424–1427.

Metzler K., Bischoff A., and Stöffler D. (1992) Accretionary dust mantles in CM chondrites: Evidence for solar nebula processes. *Geochim. Cosmochim. Acta, 56,* 2873–2897.

Möhlmann D. (1996) Origin of comets in the extended preplanetary disk. *Planet. Space Sci., 44,* 731–734.

Morfill G. E. (1983) Some cosmochemical consequences of a turbulent protoplanetary cloud. *Icarus, 53,* 41–54.

Morfill G. E., Durisen R. H., and Turner G. W. (1998) Note: An accretion rim constraint on chondrule formation theories. *Icarus, 134,* 180–184.

Morfill G. E. and Völk H. J. (1984) Transport of dust and vapor and chemical fractionation in the early protosolar cloud. *Astrophys. J., 287,* 371–395.

Mosqueira I., Kassinos S., Shariff K., and Cuzzi J. N. (2003) Hydrodynamical shear instability in accretion disks? (abstract). In *Abstracts for the 35th AAS/DPS Meeting,* Abstract #25.05.

Mukhopadyay B., Afshordi N., and Narayan R. (2005) Bypass to turbulence in hydrodynamic accretion: An eigenvalue approach. *Astrophys. J., 629,* 383–396.

Najita J., Carr J. S., and Mathieu R. D. (2003) Gas in the terrestrial planet region of disks: CO fundamental emission from T Tauri stars. *Astrophys. J., 589,* 931–952.

Nakagawa Y., Sekiya M., and Hayashi C. (1986) Settling and growth of dust particles in a laminar phase of a low-mass solar nebula. *Icarus, 67,* 375–390.

Nelson V. E. and Rubin A. E. (2002) Size-frequency distributions of chondrules and chondrule fragments in LL3 chondrites: Implications for parent-body fragmentation of chondrules. *Meteoritics & Planet. Sci., 37,* 1361–1376.

Palme H. and Fegley B. (1990) High temperature condensation of iron-rich olivine in the solar nebula. *Earth Planet. Sci. Lett., 101,* 180–195.

Papaloizou J. and Terquem C. (1999) Critical protoplanetary core masses in protoplanetary disks and the formation of short-period giant planets. *Astrophys. J., 521,* 825–838.

Paque J. and Cuzzi J. N. (1997) Physical characteristics of chondrules and rims, and aerodynamic sorting in the solar nebula (abstract). In *Lunar and Planetary Science XXVIII,* pp. 1071–1072. Lunar and Planetary Institute, Houston.

Prinn R. G. (1990) On neglect of angular momentum terms in solar nebula accretion disk models. *Astrophys. J., 348,* 725–729.

Rice W. K. M., Lodato G., Pringle J. E., Armitage P. J., and Bonnell I. A. (2004) Accelerated planetesimal growth in self-gravitating protoplanetary disks. *Mon. Not. R. Astron. Soc., 355,* 433–552.

Richard D. and Zahn J.-P. (1999) Turbulence in differentially rotating flows. What can be learned from the Couette-Taylor experiment. *Astron. Astrophys., 347,* 734–738.

Richard D. (2003) On non-linear hydrodynamic instability and enhanced transport in differentially rotating flows. *Astron. Astrophys., 408,* 409–414.

Russell S. S., Hartmann L., Cuzzi J., Krot A. N., Gounelle M., and Weidenschilling S. (2006) Timescales of the solar protoplanetary disk. In *Meteorites and the Early Solar System II* (D. S. Lauretta and H. Y. McSween Jr., eds.), this volume. Univ. of Arizona, Tucson.

Saffman P. G. and Turner J. S. (1956) On the collision of drops in turbulent clouds. *J. Fluids Mech., I,* 16; *Corrigendum, J. Fluids Mech., 196,* 599 (1988).

Safronov V. S. (1969) *Evolution of the Protoplanetary Cloud and the Formation of the Earth and Planets.* NASA TTF-677, U.S. Government Printing Office, Washington, DC.

Safronov V. S. (1991) Kuiper Prize Lecture — Some problems in the formation of the planets. *Icarus, 94,* 260–271.

Salo H. (1992) Gravitational wakes in Saturn's rings. *Nature, 359,* 619–621.

Sano T., Miyama S. M., Umebayashi T., and Nakano T. (2000) Magnetorotational instability in protoplanetary disks, II. Ionization state and unstable regions. *Astrophys. J., 543,* 486–501.

Schräpler R. and Henning Th. (2004) Dust diffusion, sedimentation, and gravitational instabilities in protoplanetary disks. *Astrophys. J., 614,* 960–978.

Scott E. R. D. and Haack H. (1993) Chemical fractionation in chondrites by aerodynamic sorting of chondritic material. *Meteoritics, 28,* 434.

Scott E. R. D., Barber D. J., Alexander C. M., Hutchison R., and Peck J. A. (1989) Primitive material surviving in chondrules: Matrix. In *Meteorites and the Early Solar System* (J. F. Kerridge and M. S. Matthews, eds.), pp. 718–745. Univ. of Arizona, Tucson.

Scott E. R. D., Love S. G., and Krot A. N. (1996) Formation of chondrules and chondrites in the protoplanetary nebula. In *Chondrules and the Protoplanetary Disk* (R. Hewins et al., eds.), pp. 87–96. Cambridge Univ., Cambridge.

Sekiya M. (1983) Gravitational instabilities in a dust-gas layer and formation of planetesimals in the solar nebula. *Prog. Theor. Phys., 69,* 1116–1130.

Sekiya M. (1998) Quasi-equilibrium density distributions of small dust aggregations in the solar nebula. *Icarus, 133,* 298–309.

Sekiya M. and Ishitsu N. (2000) Shear instabilities in the dust layer of the solar nebula I. The linear analysis of a non-gravitating one-fluid model without the Coriolis and the solar tidal forces. *Earth Planets Space, 52,* 517–526.

Sekiya M. and Ishitsu N. (2001) Shear instabilities in the dust layer of the solar nebula II. Different unperturbed states. *Earth Planets Space, 53,* 761–765.

Sekiya M. and Takeda H. (2003) Were planetesimals formed by dust accretion in the solar nebula? *Earth Planets Space, 55,* 263–269.

Shakura N. and Sunyaev R. A. (1973) Black holes in binary systems. Observational appearance. *Astron. Astrophys., 24,* 337–355.

Shakura N. I., Sunyaev R. A., and Zilitinkevich S. S. (1978) On the turbulent energy transport in accretion disks. *Astron. Astrophys., 62,* 179–187.

Shu F. H., Shang H., and Lee T. (1996) Toward an astrophysical theory of chondrites. *Science, 271,* 1545–1552.

Shu F. H., Shang H., Glassgold A. E., and Lee T. (1997) X-rays and fluctuating X-winds from protostars. *Science, 277,* 1475–1479.

Sirono S. and Greenberg J. M. (2000) Do cometesimal collisions lead to bound rubble piles or to aggregates held together by gravity? *Icarus, 145,* 230–238.

Skinner W. R. (1990a) Bipolar outflows and a new model of the early solar system. Part I: Overview and implications of the model (abstract). In *Lunar and Planetary Science XXI,* p. 1166. Lunar and Planetary Institute, Houston.

Skinner W. R. (1990b) Bipolar outflows and a new model of the early solar system. Part II: The origins of chondrules, isotopic anomalies, and fractionations (abstract). In *Lunar and Planetary Science XXI,* p. 1168. Lunar and Planetary Institute, Houston.

Skinner W. R. and Leenhouts J. M. (1991) Implications of chondrule sorting and low matrix contents of type 3 ordinary chondrites. *Meteoritics, 26,* 396.

Skinner W. R. and Leenhouts J. M. (1993) Size distributions and aerodynamic equivalence of metal chondrules and silicate chondrules in Acfer 059 (abstract). In *Lunar and Planetary Science XXIV,* pp. 1315–1316. Lunar and Planetary Institute, Houston.

Squires K. D. and Eaton J. A. (1990) particle response and turbulence modification in isotropic turbulence. *Phys. Fluids, A2,* 1191–1203.

Squires K. D. and Eaton J. A. (1991) Preferential concentration of particles by turbulence. *Phys. Fluids, A3,* 1169–1178.

Sreenivasan K. R. and Stolovitsky K. (1995a) Intermittency, the second-order structure function, and the turbulent energy dissipation rate. *Phys. Rev. E, 52,* 3242–3244.

Sreenivasan K. R. and Stolovitsky K. (1995b) Turbulent cascades. *J. Stat. Phys., 78,* 311–333.

Stepinski T. F. and Valageas P. (1996) Global evolution of solid matter in turbulent protoplanetary disks. I. Aerodynamics of solid particles. *Astron. Astrophys., 309,* 301–312.

Stepinski T. F. and Valageas P. (1997) Global evolution of solid matter in turbulent protoplanetary disks. II. Development of icy planetesimals. *Astron. Astrophys., 319,* 1007–1019.

Stevenson D. J. and Lunine J. I. (1988) Rapid formation of Jupiter by diffuse redistribution of water vapor in the solar nebula. *Icarus, 75,* 146–155.

Stone J. M., Gammie C. F., Balbus S. A., and Hawley J. F. (2000) Transport processes in protostellar disks. In *Protostars and Planets IV* (V. Mannings et al., eds.), pp. 589–599. Univ. of Arizona, Tucson.

Supulver K. and Lin D. N. C. (2000) Formation of icy planetesimals in a turbulent solar nebula. *Icarus, 146,* 525–540.

Tanga B. A., Dubrulle B., and Provenzale A. (1996) Forming planetesimals in vortices. *Icarus, 121,* 158–170.

Tanga P., Weidenschilling S. J., Michel P., and Richardson D. C. (2004) Gravitational instability and clustering in a disk of planetesimals. *Astron. Astrophys., 427,* 1105.

Tennekes H. and Lumley J. L. (1972) *A First Course in Turbulence.* Massachusetts Institute of Technology, Cambridge. 300 pp.

Thompson J. J. and Newhall H. F. (1885) On the formation of vortex rings by drops falling into liquids, and some allied phenomena. *Proc. R. Soc., 39,* 417.

Toomre A. (1964) On the gravitational stability of a disk of stars. *Astrophys. J., 139,* 1217–1238.

Trieloff M., Jessberger E. K., Herrwerth I., Hopp J., Fiéni C., Ghéllis M., Bourot-Denis M., and Pellas P. (2003) Surface and thermal history of the H-chondrite parent asteroid revealed by thermochronometry. *Nature, 422,* 502–506.

Umurhan O. M. and Regev O. (2004) Hydrodynamic stability of rotationally supported flows: Linear and nonlinear 2D shearing box results. *Astron. Astrophys., 427,* 855–872.

Völk H. J., Jones F. C., Morfill G. E., and Röser S. (1980) Collisions between grains in a turbulent gas. *Astron. Astrophys., 85,* 316–325.

Wang L. and Maxey M. R. (1993) Settling velocity and concentration distribution of heavy particles in homogeneous isotropic turbulence. *J. Fluids Mech., 256,* 27–68.

Ward W. R. (2000) On planetesimal formation: The role of collective particle behavior. In *Origin of the Earth and Moon* (R. M. Canup and K. Righter, eds.), pp. 75–84. Univ. of Arizona, Tucson.

Wasson J. T., Trigo-Rodriguez J. M., and Rubin A. E. (2005) Dark mantles around CM chondrules are not accretionary rims (abstract). In *Lunar and Planetary Science XXXVI,* Abstract #2314. Lunar and Planetary Institute, Houston (CD-ROM).

Weidenschilling S. J. (1977) Aerodynamics of solid bodies in the solar nebula. *Mon. Not. R. Astron. Soc., 180,* 57–70.

Weidenschilling S. J. (1980) Dust to planetesimals: Settling and coagulation in the solar nebula. *Icarus, 44,* 172–189.

Weidenschilling S. J. (1984) Evolution of grains in a turbulent solar nebula. *Icarus, 60,* 553–567.

Weidenschilling S. J. (1988a) Formation processes and timescales for meteorite parent bodies. In *Meteorites and the Early Solar*

*System* (J. F. Kerridge and M. S. Matthews, eds.), pp. 348–371. Univ. of Arizona, Tucson.

Weidenschilling S. J. (1988b) Dust to dust: Low-velocity impacts of fragile projectiles (abstract). In *Lunar and Planetary Science XIX*, pp. 1253–1254. Lunar and Planetary Institute, Houston.

Weidenschilling S. J. (1995) Can gravitational instability form planetesimals? *Icarus, 116,* 433–435.

Weidenschilling S. J. (1997) The origin of comets in the solar nebula: A unified model. *Icarus, 127,* 290–306.

Weidenschilling S. J. (2000) Formation of planetesimals and accretion of the terrestrial planets. *Space Sci. Rev., 92,* 295–310.

Weidenschilling S. J. (2003a) Radial drift of particles in the solar nebula: Implications for planetesimal formation. *Icarus, 165,* 438–442.

Weidenschilling S. J. (2003b) Planetesimal formation in two dimensions: Putting an edge on the solar system (abstract). In *Lunar and Planetary Science XXXIV*, Abstract #1707. Lunar and Planetary Institute, Houston (CD-ROM).

Weidenschilling S. J. (2006) Accretion dynamics and timescales: Relation to chondrites. In *Meteorites and the Early Solar System II* (D. S. Lauretta and H. Y. McSween Jr., eds.), this volume. Univ. of Arizona, Tucson.

Weidenschilling S. and Cuzzi J. N. (1993) Formation of planetesimals in the solar nebula. In *Protostars and Planets III* (E. Levy and J. Lunine, eds.), pp. 1031–1060. Univ. of Arizona, Tucson.

Weisberg M. K., McCoy T. J., and Krot A. N. (2006) Systematics and evaluation of meteorite classification. In *Meteorites and the Early Solar System II* (D. S. Lauretta and H. Y. McSween Jr., eds.), this volume. Univ. of Arizona, Tucson.

Whipple F. (1972) On certain aerodynamic processes for asteroids and comets. In *From Plasma to Planet* (A. Elvius, ed.), pp. 211–232. Wiley, New York.

Wilcox D. (1998) *Turbulence Modeling for CFD, 2nd edition*, Chapter 3. DCW Industries, Inc., La Canada, California.

Wood J. A. (1985) Meteoritic constraints on processes in the solar nebula. In *Protostars and Planets II* (D. C. Black and M. S. Matthews, eds.), pp. 687–702. Univ. of Arizona, Tucson.

Wood J. A. (2000) Pressure and temperature profiles in the solar nebula. *Space Sci. Rev., 92,* 87–93.

Wood J. A. (2004) Formation of chondritic refractory inclusions: The astrophysical setting. *Geochim. Cosmochim. Acta, 68,* 4007–4021.

Wood J. A. and Morfill G. E. (1988) A review of solar nebula models. In *Meteorites and the Early Solar System* (J. F. Kerridge and M. S. Matthews, eds.), pp. 329-347. Univ. of Arizona, Tucson.

Woolum D. and Cassen P. (1999) Astronomical constraints on nebular temperatures: Implications for planetesimal formation. *Meteoritics & Planet. Sci., 34,* 897–907.

Wurm G., Blum J., and Colwell J. (2001) A new mechanism relevant to the formation of planetesimals in the solar nebula. *Icarus, 151,* 318–321.

Yamoto F. and Sekiya M. (2004) The gravitational instability in the dust layer of a protoplanetary disk: Axisymmetric solutions for nonuniform dust density distributions in the direction vertical to the midplane. *Icarus, 170,* 180–192.

Youdin A. and Shu F. (2002) Planetesimal formation by gravitational instability. *Astrophys. J., 580,* 494–505.

Youdin A. N. and Chiang E. I. (2004) Particle pileups and planetesimal formation. *Astrophys. J., 601,* 1109–1119.

Yurimoto H. and Kuramoto N. (2004) Molecular cloud origin for the oxygen isotope heterogeneity in the solar system. *Science, 305,* 1763–1766.